Journal of Geodynamics xxx (2016) xxx–xxx

Contents lists available at ScienceDirect

Journal of Geodynamics

journal homepage: http://www.elsevier.com/locate/jog

Early Earth plume-lid tectonics: A high-resolution 3D numerical modelling approach

R. Fischer*, T. Gerya

Geophysical Fluid Dynamics Group, Institute of Geophysics, Department of Earth Sciences, Swiss Federal Institute of Technology (ETH-Zurich), Sonneggstrasse, 5, 8092 Zurich, Switzerland

ARTICLE INFO

Article history:
Received 28 September 2015
Received in revised form 4 March 2016
Accepted 9 March 2016
Available online xxx

Keywords:
Precambrian
Archean
Plume-lid tectonics
Subduction
Hadean

ABSTRACT

Geological–geochemical evidence point towards higher mantle potential temperature and a different type of tectonics (global plume-lid tectonics) in the early Earth (>3.2 Ga) compared to the present day (global plate tectonics). In order to investigate tectono-magmatic processes associated with plume-lid tectonics and crustal growth under hotter mantle temperature conditions, we conduct a series of 3D high-resolution magmatic-thermomechanical models with the finite-difference code I3ELVIS. No external plate tectonic forces are applied to isolate 3D effects of various plume–lithosphere and crust–mantle interactions. Results of the numerical experiments show two distinct phases in coupled crust–mantle evolution: (1) a longer (80–100 Myr) and relatively quiet 'growth phase' which is marked by growth of crust and lithosphere, followed by (2) a short (~20 Myr) and catastrophic 'removal phase', where unstable parts of the crust and mantle lithosphere are removed by eclogitic dripping and later delamination. This modelling suggests that the early Earth plume-lid tectonic regime followed a pattern of episodic growth and removal also called episodic overturn with a periodicity of ~100 Myr.

1. Introduction

In the late 18th century the famous Scottish geologist, James Hutton – father of modern geology – introduced the idea of uniformitarianism. He understood that the land we see today was shaped by processes that had acted in a similar fashion in the past and will continue to act in the same manner (Hutton, 1788). In the early 19th century Sir Charles Lyell rephrased this idea into what is still taught to geology students all around the globe: "The present is the key to the past". The uniformitarian view is holding up well to explain modern geodynamics and the successful paradigm of plate tectonics through the Phanerozoic. But gradual changes appear in the style of tectonics through the Proterozoic and late Archean (Sizova et al., 2010, 2014; O'Neill and Wyman, 2013; Fischer and Gerya, submitted for publication), and controversy remains for the early Archean, >3.2 Ga.

From our present-day understanding of geodynamics, however, we struggle to understand processes older than 3.2 Ga (Champion and Smithies, 2007; Van Kranendonk et al., 2007; Gerya, 2014a, and references therein), such as the formation of cratons or even the dominant tectonic style in the Hadean and early Archean. What is needed is a global working paradigm for Archean geodynamics comparable to plate tectonics (Benn et al., 2006). The directly accessible surface rock record of early Archean age is sparse and unaltered geophysical data is limited, which amplifies the role of quantitative geodynamic modelling approaches for the integration of observational constraints from a wide range of disciplines in order to further our understanding of Archean geodynamics (Champion and Smithies, 2007; Van Kranendonk et al., 2007; Gerya, 2014a and references therein).

From the perspective of numerical geodynamic modelling present day geodynamics, plate tectonics, are predominantly driven by tectonism. Tectonism is a process of deformation in the Earth's crust that produces its continents and ocean basins, plateaus and mountains, fold of strata, and faults. Thermomechanical models are therefore sufficient to understand modern geodynamics. In the early Earth, however, the increased mantle temperature leads to massive heat and mass advection by mantle-derived magmas and widespread melt-induced weakening of the lithosphere (Lenardic et al., 2005; Gerya et al., 2015 and references therein). Archean geodynamics follow an overall tectono-magmatic style and require more sophisticated magmatic-thermomechanical models (Sizova et al., 2015).

Several different models have already been proposed to describe Archean tectonics. For example, it has been suggested that the Archean Earth and its tectonic style was similar to present-day

* Corresponding author.
E-mail address: ria.fischer@erdw.ethz.ch (R. Fischer).

http://dx.doi.org/10.1016/j.jog.2016.03.004
0264-3707/

Venus (e.g. Van Kranendonk, 2010; Harris and Bédard, 2014, 2015). These authors argue that the two planets are relatively similar in many ways, however, Venus has preserved not only a higher surface temperature but also a higher internal temperature due to its closer distance to the sun (Breuer and Moore, 2007). Venusian surface tectonics is marked by an absence of a well-defined plate mosaic and by the presence of striking coronae and novae features (Hansen and Willis, 1996; Phillips and Hansen, 1998; Gerya, 2014b, and references therein). The common theory is that these features are formed by mantle plumes and that the planet experiences episodic overturn events rather than the style of plate tectonics that we observe on present day Earth (Schaber et al., 1992; Strom et al., 1994; Armann and Tackley, 2012). Observed large displacements of plana are speculated to be driven by mantle flow (Harris and Bédard, 2015).

The hypothesis of plume-induced tectonics, plume-lid tectonics (Gerya et al., 2015), is often invoked for the early Archean. In this case, tectonic deformation of crust and lithosphere is not produced by plate tectonics and its major driving forces, among others the slab pull force (van Hunen and Moyen, 2012), but by mantle plumes and various other active mantle and crustal upwellings and downwellings. The Archean plume-lid tectonics regime was described by Van Kranendonk (2011b), who suggested an early Earth geodynamic style (before 3 Ga) with small mobile plates and rapid upper mantle convection. Continental crust is formed by volcanism over upwelling mantle or by imbrication over downwelling mantle (Van Kranendonk, 2011b). Johnson et al. (2014) and Sizova et al. (2015) modelled early Earth plume-lid tectonics in 2D, where they showed that continued melting and dripping of over-thickened crust under Archean conditions in combination with fractionation could lead to the necessary source magmas for TTG melts. van Thienen et al. (2005) discussed 2D models of the whole mantle under Archean conditions, concluding that the Archean mantle shows strong heterogeneity and different reservoirs produced by convective instabilities and resurfacing events.

Crustal and mantle processes associated with plume–lithosphere interactions are intrinsically three-dimensional and require 3D numerical modelling approaches (Burov and Gerya, 2014). Therefore, a systematic 3D high-resolution magmatic-thermomechanical numerical modelling effort is required to understand how plume-lid tectonics operated in the early Earth. In our previous study (Fischer and Gerya, submitted for publication) we investigated a gradual change between the two global tectonic regime end-members, present day plate tectonics and Archean plume-lid tectonics with increasing mantle potential temperature using kinematically driven 3D models with typical present-day oceanic-continental plate boundary settings. In contrast, this new study will focus on the plume-lid tectonics regime itself, based on more appropriate 3D magmatic-thermomechanical models with laterally homogeneous unstressed lithosphere (Johnson et al., 2014; Sizova et al., 2015).

2. Methods

2.1. Model design

In order to investigate tectono-magmatic processes associated with plume-lid tectonics and crustal growth under hot Archean mantle temperature conditions we investigate a series of 3D high-resolution magmatic-thermomechanical models. In contrast to our previous study (Fischer and Gerya, submitted for publication), no external plate tectonic forces were applied in these models in order to isolate 3D effects of plume–lithosphere and crust–mantle interactions (Johnson et al., 2014; Sizova et al., 2015; Fischer and Gerya, submitted for publication).

2.1.1. Initial and boundary conditions

To model Archean upper mantle and crustal processes, a model setup of 520 km in length, width and depth has been chosen. The initial laterally homogeneous plate setup Fig. 1a is simplified to prevent inscription of any predefined structures and consists of a 35 km thick crust of varying composition (Table 2) on top of the asthenospheric mantle.

We use the 3D numerical magmatic-thermomechanical I3ELVIS code (Gerya and Yuen, 2007) which is based on a conservative finite difference method with a multigrid solver and a non-diffusive marker-in-cell technique to simulate multiphase flow (Gerya and Yuen, 2003, 2007). Additionally, the 3D code features melting of crustal and mantle rocks and volcanic and plutonic addition of juvenile crust from extracted mantle-derived melt, eclogitic phase changes as well as hydration and dehydration processes (Zhu et al., 2013; Gerya et al., 2015).

The crust is chosen either one- or two-layered, following Van Kranendonk et al. (2014) for a 'Stage 1: developing protocrust'. In the two-layered case, both layers are initially chosen to be 17.5 km thick. Various crustal compositions are explored, one- and two-layered felsic crust and one- and two-layered mafic crust as well as felsic rocks underlain by mafic crust (Table 2; Rudnick and Gao, 2003).

All velocity boundary conditions are free slip. The uppermost 20 km of the model domain is filled with 'sticky air' which acts as an internal free surface boundary condition (Crameri et al., 2012). In order to ensure mantle plume growth from the bottom of the model (Johnson et al., 2014; Sizova et al., 2015) an elevated mantle temperature of 2313 K is prescribed at the lower boundary which is 240 K higher than the potential mantle temperature at this depth.

A highly simplified instantaneous erosion and sedimentation model is implemented. Rock markers of any type which are found above the erosion level $y_{eroslev}$ = 10 km are eroded instantaneously. In a independent sedimentation process trenches below the sedimentation layer $y_{sedilev}$ = 25 km are filled instantaneously and converted to layered sediments. The sea level is fixed at $y_{waterlev}$ = 20 km.

The initial temperature structure of the model is adjusted to the Archean Earth (Fischer and Gerya, submitted for publication; Sizova et al., 2010, 2015; Brown, 2007). According to Herzberg et al. (2010) a elevated mantle potential temperature of T_p = 1823 K can occur at any age >1.5 Ga. However, comparison of modelling results with geological observations (e.g., Collins et al., 1998; Van Kranendonk, 2011a) shows that the appropriate time range is closer to early Archean. The crust has a hot initial geotherm with a fixed temperature of 273 K at the top. The uppermost 10 km have a temperature gradient of 100 K/km, the next 20 km have a lower temperature gradient of 5 K/km. The following layer of 10 km thickness and a temperature gradient of 47 K/km acts as transition between crust and asthenospheric mantle.

In the initial model no lithosphere is defined either thermally or compositionally. However, lithosphere is able to develop spontaneously through the course of the model. The asthenospheric mantle has a linear adiabatic temperature gradient of 0.5 K/km and the mantle potential temperature T_p is increased by ΔT_p = 267 K compared to present day reference mantle potential temperature $T_p = T_{initial}$ = 1556 K. A pre-existing self-consistent mantle depletion profile is defined, that corresponds to dry melting along the prescribed mantle potential temperature profile with an adiabatic thermal gradient of 0.5 K/km. The lowermost 40 km at the model bottom have a steep temperature gradient to meet the increased thermal boundary condition of 2313 K. As an initial thermal perturbation in the mantle, a half-sphere of 40 km radius is inscribed with a temperature of 2313 K at the centre of the lower boundary (Fig. 1a).

Please cite this article in press as: Fischer, R., Gerya, T., Early Earth plume-lid tectonics: A high-resolution 3D numerical modelling approach. J. Geodyn. (2016), http://dx.doi.org/10.1016/j.jog.2016.03.004

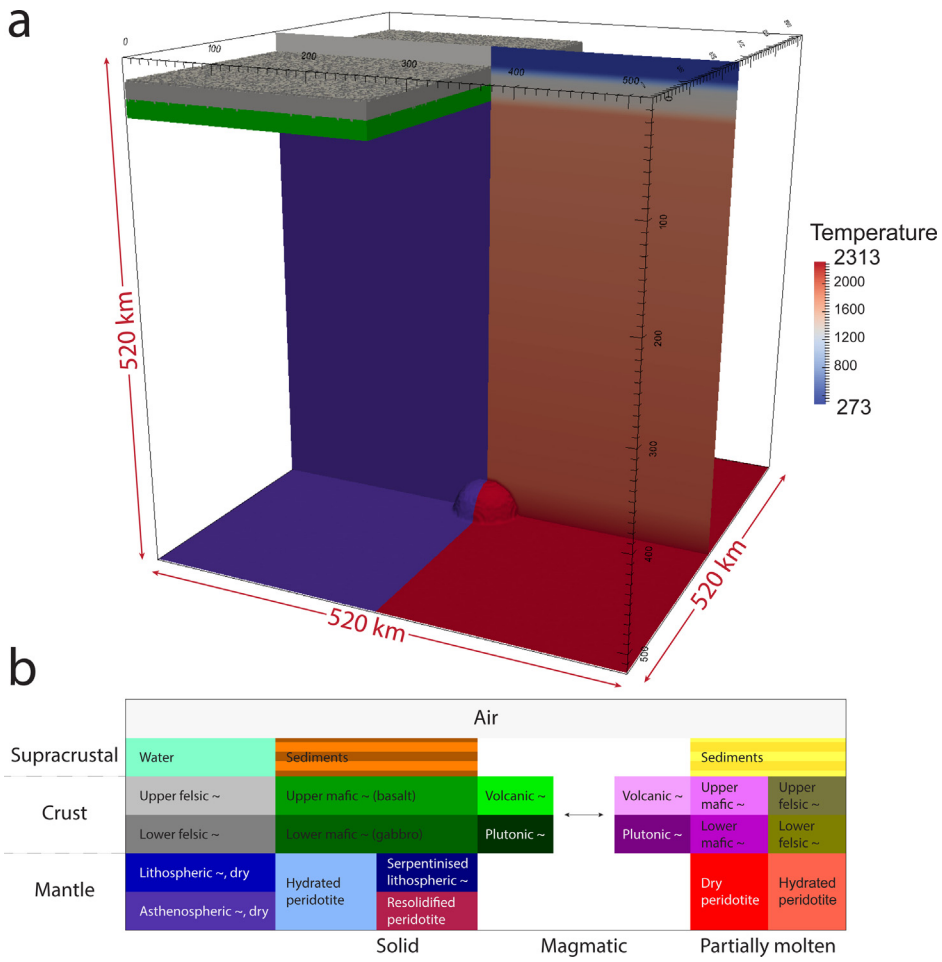

Fig. 1. (a) The initial model setup shown in 3D as well as a 2D cross-section. The left side shows the initial compositional setup whereas the right side shows the initial temperature structure. (b) All available material types and their colour code in both solid and partially molten state as will be used throughout this paper.

2.1.2. Modelling of dehydration, hydration and water transport

The hydration and dehydration model is based on the water markers approach (Gerya and Meilick, 2011). The equilibrium mineralogical water content is computed for the crust and the mantle as a function of pressure and temperature from thermodynamic data by free energy minimization (Connolly, 2005; Gerya and Meilick, 2011). In addition, water is present as pore fluid with concentrations of up to 2 wt% in the crust. The pore water content $X_{H_2O}(P)$ (wt%) decreases linearly from the maximal value of $X_{H_2O}(P_0) =$ 2 wt% at the surface to 0 wt% at 75 km depth.

2.1.3. Modelling of melting and crustal growth

In order to account for changes in melting conditions (e.g., solidus and liquidus temperatures – $T_{solidus}$ and $T_{liquidus}$) with varying rock composition, four different melting models are used. For sediments and felsic rocks like dry or hydrated upper continental crust a granite melting model is applied (Johannes, 1985; Poli and Schmidt, 2002; Gerya et al., 2006). For all hydrated mafic rocks like upper oceanic crust, hydrated lower continental crust and new formed volcanic rocks a basalt melting model is applied (Schmidt and Poli, 1998; Hess, 1989; Gerya et al., 2006). A gabbro melting model (Hess, 1989; Gerya et al., 2006) is applied to the lower part of both oceanic and continental crust. For mantle peridotite in various stages of hydration a P-T-H_2O dependent melting model (Katz et al., 2003) is applied. Dry mantle melting is only activated at pressures less than a maximum pressure $P_{max} = 10$ GPa to avoid unrealistic results arising from the extrapolating melting model. See Table 1 material properties and melting parameters.

For all crustal lithologies, the standard melt fraction is calculated according to a simplified linear melting model (Gerya et al., 2006),

$$M_0 = \begin{cases} 0, & \text{if } T < T_{solidus} \\ \dfrac{T - T_{solidus}}{T_{liquidus} - T_{solidus}}, & \text{if } T_{solidus} < T < T_{liquidus} \\ 1, & \text{if } T > T_{liquidus} \end{cases} \quad (1)$$

where M_0 is the standard volumetric degree of melting before melt extraction. For the mantle, the non-linear melting model of Katz et al. (2003) is used to calculate M_0. In mantle rocks, the actual amount of melt M is defined as the difference between the standard melt fraction M_0 and the amount of previously extracted melt $\sum_n M_{ext}$ which is accumulated for each marker in the course of the model where n is the number of melt extraction episodes:

$$M = M_0 - \sum_n M_{ext}. \quad (2)$$

To simulate melt extraction from mantle rocks an extraction threshold $M_{max} = 4$ wt% is defined. If the total amount of melt M on a marker surpasses this threshold (i.e. when $M > M_{max}$) all melt except for a non-extractable part $M_{min} = 2$ wt% is extracted: $\sum_{n+1} M_{ext} = \sum_n M_{ext} + M - M_{min}$. The amount of extracted melt is then instantaneously transported upwards and randomly chosen to be deposited as either volcanic or plutonic crust, thereby keeping a prescribed eruption efficiency (i.e., a volcanic rock fraction, $0\% < \chi_{volc} < 100\%$). Volcanic rocks are deposited at the surface while plutonic rocks are deposited at the Moho. At the beginning of the

Please cite this article in press as: Fischer, R., Gerya, T., Early Earth plume-lid tectonics: A high-resolution 3D numerical modelling approach. J. Geodyn. (2016), http://dx.doi.org/10.1016/j.jog.2016.03.004

Table 1
Material properties [a] as well as applied rheology and melting model is listed for each of the used lithologies as given in Fig. 1a.

Material	Rheology [$MPa^{-n}\,s^{-1}$], [–], [kJ], [J/bar]	ρ_0 [kg/m^3]		k [K]	Melting [W/m K]	H_r [$\mu W/m^3$]	H_L [kJ/kg]	ϕ_0, ϕ_1 [–]	γ_0, γ_1 [–]	σ_{crit} [MPa]	C_p [kJ/kg]
Sediments	Wet quartzite flow law	2600	Solid	$0.64+\frac{807}{T+77}$	Granite	2.0	–	0.0,0.0	0.0,0.5	0.03	1.0
	$B_D = 1.97\times10^{17}$, $n=2.3$,	2400	Molten			2.0	300	–	–	–	1.5
Upper felsic crust	$E_a = 154$, $V_a = 0$	2750	Solid			1.0	–	0.200,0.0	0.0,0.5	0.03	1.0
		2400	Molten	-//-	-//-	2.0	300	–	–	–	1.5
Hydrated felsic crust		2700	Solid			1.0	–	0.200,0.0	0.0,0.5	0.03	1.0
	-//-	2400	Molten			1.0	300	–	–	–	1.5
Upper mafic crust		3000	Solid	$1.18+\frac{474}{T+77}$	Basalt	0.25	–	0.0,0.0	0.0,0.5	0.03	1.0
		2900	Molten	$0.64+\frac{807}{T+77}$		0.25	380	–	–	–	1.5
Volcanic crust		3000	Solid	$1.18+\frac{474}{T+77}$	-//-	0.25	–	0.0,0.0	0.0,0.5	0.03	1.0
		2900	Molten	-//-		0.25	380				1.5
Lower felsic crust	Plagioclase An_{75} flow law	2950	Solid	$1.18+\frac{474}{T+77}$	Gabbro	0.5	–	0.200,0.0	0.0,0.5	0.03	1.0
	$B_D = 4.80\times10^{22}$, $n=3.2$,	2400	Molten	$0.64+\frac{807}{T+77}$		2.0	380	–	–	–	1.5
Lower mafic crust	$E_a = 238$, $V_a = 0$	3000	Solid	$1.18+\frac{474}{T+77}$	-//-	0.25	–	0.200,0.0	0.0,0.5	0.03	1.0
		2900	Molten			0.25	380	–	–	–	1.5
Plutonic crust		3000	Solid	-//-	Basalt	0.25	–	0.200,0.0	0.0,0.5	0.03	1.0
	-//-	2900	Molten			0.25	380	–	–	–	1.5
Hydrated crust		2900	Solid		-//-	0.5	–	0.200,0.0	0.0,0.5	30	1.0
		2400	Molten	$0.64+\frac{807}{T+77}$		1.0	380	–	–	–	1.5
Asthenospheric mantle	Dry olivine flow law	3300	Solid	$0.73+\frac{1293}{T+77}$	Peridotite	0.022	–	0.200,0.0	0.0,0.5	0.03	1.0
	$B_D = 3.98\times10^{16}$, $n=3.5$,	2900	Molten			0.023	400	–	–	–	1.5
Depleted mantle	$E_a = 532$, $V_a = 0.8$	3300	Solid			0.020	–	0.200,0.0	0.0,0.5	0.03	1.0
		2900	Molten	-//-	-//-	0.021	400	–	–	–	1.5
Quenched mantle	-//-	3300	Solid			0.024	–	0.200,0.0	0.0,0.5	0.03	1.0
		2900	Molten			0.025	400	–	–	–	1.5
Hydrated mantle	Wet olivine flow law	3300	Solid	$0.73+\frac{1293}{T+77}$	Peridotite	0.024	–	0.200,0.0	0.0,0.5	30	1.0
	$B_D = 5.01\times10^{20}$, $n=4.0$,	2900	Molten		-//-	0.025	400	–	–	–	1.5
Serpentinite	$E_a = 470$, $V_a = 0.8$	3300	Solid	-//-	–	0.024	–	0.200,0.0	0.0,0.5	30	1.0
References[b]	4,1	1,2		3	5–10	1	1, 2				

[a] For all rock types: cohesion $C_0 = C_1 = 1$ MPa. Thermal expansion coefficient $\alpha = 3.0\times10^{-5}\,K^{-1}$ and compressibility $\beta = 1.0\times10^{-5}\,GPa^{-1}$.
[b] (1) Turcotte and Schubert (2002), (2) Bittner and Schmeling (1995), (3) Clauser and Huenges (1995), (4) Ranalli (1995), (5) Schmidt and Poli (1998), (6) Johannes (1985), (7) Poli and Schmidt (2002), (8) Schmidt and Poli (1998), (9) Hess (1989), (10) Katz et al. (2003).

model when no lithosphere exists yet, the Moho is equal to the lithosphere–asthenosphere boundary (LAB).

Eruption efficiency of volcanic against plutonic eruption can be freely varied via the parameter χ_{volc}. Eruption efficiency on present-day Earth is estimated to be around 5–20% (Crisp, 1984). However, it is not clear whether this also holds true for Archean tectonic settings. In the heat-pipe mode suggested by Moore and Webb (2013) it is assumed to be 100%. We therefore vary χ_{volc} between 0% and 100% (see Table 2).

2.1.4. Density changes due to phase transitions and mantle depletion

For the basalts of the upper and lower mafic crust a phase transition from basalt to garnet-granulite and then eclogite (Ito and Kennedy, 1971) is applied. Eclogitization of the crust is implemented as a linear density increase with pressure and temperature from 0% to 16% in the P–T region between the experimentally determined garnet-in and plagioclase-out phase transitions in basalt (Ito and Kennedy, 1971). For temperatures lower than $t_{ecl_{min}} = 673$ K no eclogitization is possible. For temperatures between $t_{ecl_{min}}$ and $t_{ecl_{max}} = 873$ K the maximum density increase due to eclogitization is linearly increasing with temperature from 0% to 16%.

Depending on the accumulated amount of extracted melt $\sum_n M_{ext}$ (i.e. with increasing degree of mantle depletion) the density of solid peridotite and solid fraction of partially molten peridotite decreases (Schutt and Lesher, 2006).

$$\rho_{s(depleted)} = \rho_s \cdot \left(1.0 - 0.04 \cdot \sum_{n-1} M_{ext}\right). \quad (3)$$

For mantle peridotite with an accumulated amount of extracted melt $\sum_n M_{ext} > 0.3$ the mantle is visualized as lithospheric (depleted) instead of asthenospheric (fertile) peridotite (cf. Fig. 1b for the colour code). However, further depletion is still possible.

Table 2
List of all reference models. All models are designed using the setup described in Section 2.1.1 and Fig. 1a.

Model	χ_{volc} [%]	$\dot{\varepsilon}_{healing}$ [s^{-1}]	λ_{melt}	Upper crust	Lower crust
A20	20	10^{-14}	0.01	Felsic wet	Felsic dry
B20	20	10^{-14}	0.01	Felsic wet	Mafic dry
B100b	100	0	1.0	Felsic wet	Mafic dry
C20	20	10^{-14}	0.01	Mafic wet	Mafic dry
D0	0	10^{-14}	0.01	Mafic dry	
D0b	0	2.5×10^{-14}	0.0	Mafic dry	
D20	20	10^{-14}	0.01	Mafic dry	
D100	100	10^{-14}	0.01	Mafic dry	
D100b	100	0	1.0	Mafic dry	
E100b	100	0	1.0	Felsic wet	

2.1.5. Rheological model

14 different rock types (not including 'sticky air' and 'sticky water') are available in both solid and partially molten state (see Fig. 1b). Four different visco-plastic flow laws are applied to these rock types. A wet quartzite flow law (Ranalli, 1995) is applied to sediments and upper crustal material. The lower crust follows a plagioclase An_{75} flow law and dry or wet mantle follow a respective (i.e., dry or wet) olivine flow law (Ranalli, 1995). See Table 1 for a full compilation of material properties (and Table S1 for models *B100b*, *D0b*, *D100b* and *E100b*).

A visco-plastic rheology is employed, where the relationship between the deviatoric stress σ'_{ij} and strain-rate $\dot{\varepsilon}_{ij}$ is described by the visco-plastic constitutive law.

Please cite this article in press as: Fischer, R., Gerya, T., Early Earth plume-lid tectonics: A high-resolution 3D numerical modelling approach. J. Geodyn. (2016), http://dx.doi.org/10.1016/j.jog.2016.03.004

For the ductile creep regime, contributions from different flow laws such as dislocation and diffusion creep are taken into account using the inverse effective ductile viscosity $\eta_{ductile}$:

$$\frac{1}{\eta_{ductile}} = \frac{1}{\eta_{newt}} + \frac{1}{\eta_{powl}}, \tag{4}$$

where η_{newt} and η_{powl} are effective viscosities for Newtonian diffusion and power-law dislocation creep, respectively.

In high stress regions where $\sigma_{II} > 10^8$ Pa the Peierls creep mechanism is invoked additionally, with a maximum strength of the material, the dry Peierls stress $\sigma_{Peierls} = 9.1 \times 10^9$ Pa, similar to the yield stress (Katayama and Karato, 2008). η_{Peirls} is the Peierls viscosity, which is computed for this plastic creep.

A brittle Drucker–Prager yield criterion with strain weakening and fracture healing is implemented (following Gerya, 2013, and references therein). For brittle or plastic deformation a yield stress σ_{yield} is defined, which depends on the cohesion C_γ, the internal friction coefficient ϕ_γ, and the melt-induced weakening factor λ_{melt}. The melt-induced weakening factor itself depends on the melt pressure P_{melt} and the total pressure P.

$$\sigma_{yield} = C_\gamma + \phi_\gamma P \lambda_{melt}, \tag{5a}$$

$$\lambda_{melt} = 1 - \frac{P_{melt}}{P}, \tag{5b}$$

Melt-induced weakening (see Table 2) is only applied locally to lithospheric rock markers above areas of melt extraction. For all other rocks no weakening is assumed ($\lambda_{melt} = 1$).

Internal friction angle ϕ_γ and cohesion C_γ are defined as follows:

$$\phi_\gamma = \begin{cases} \phi_0, & \text{if } \gamma \le \gamma_0 \\ \phi_0 + (\phi_1 - \phi_0)\dfrac{\gamma - \gamma_0}{\gamma_1 - \gamma_0}, & \text{if } \gamma_0 < \gamma \le \gamma_1 \\ \phi_1, & \text{if } \gamma > \gamma_1, \end{cases} \tag{6}$$

$$C_\gamma = \begin{cases} C_0, & \text{if } \gamma \le \gamma_0 \\ C_0 + (C_1 - C_0)\dfrac{\gamma - \gamma_0}{\gamma_1 - \gamma_0}, & \text{if } \gamma_0 < \gamma \le \gamma_1 \\ C_1, & \text{if } \gamma > \gamma_1, \end{cases} \tag{7}$$

where ϕ_0 and ϕ_1 are the initial and final values for the friction angle, C_0 and C_1 are the initial and final values for the cohesion, $\gamma \ge 0$ is the integrated plastic strain and γ_0 and γ_1 are the lower and upper strain limits for fracture related weakening respectively. Values for all different rock types can be found in Table 1. The integrated plastic strain γ is calculated in the following way:

$$\gamma = \int \sqrt{\frac{1}{2}\dot{\varepsilon}^2_{ij(plastic)}}\,dt - \int \dot{\varepsilon}_{healing}\,dt, \tag{8}$$

where $\dot{\varepsilon}_{ij(plastic)}$ is the plastic strain rate tensor and $\dot{\varepsilon}_{healing}$ is the fracture healing rate (see Table 2).

An upper viscosity limit $\eta_{plastic}$ of the yielding material can now be calculated by using the second invariant of the strain rate tensor $\dot{\varepsilon}_{II} = \sqrt{1/2\dot{\varepsilon}^2_{ij}}$:

$$\eta_{plastic} = \frac{\sigma_{yield}}{2\dot{\varepsilon}_{II}}, \tag{9}$$

The effective viscosity $\eta_{eff}(T, P, c, M)$ is the minimum of all viscosity values,

$$\frac{1}{\eta_{eff}} = \max\left\{\frac{1}{\eta_{ductile}}, \frac{1}{\eta_{Peierls}}, \frac{1}{\eta_{plastic}}\right\}. \tag{10}$$

We use 10^{18} Pa s and 10^{24} Pa s as respectively lower and upper cut-off viscosity limits for all types of materials.

2.2. Reference model series

According to Sizova et al. (2010), Fischer and Gerya (submitted for publication) the increase in mantle potential temperature ΔT_p is the major parameter which influences transition from plume tectonics to plate tectonics. At high $\Delta T_p = 250$ K no elements of plate tectonics are visible. To explore the plume tectonic end-member we therefore assume an increase in mantle potential temperature of $\Delta T_p = 267$ K while assuming a present day mantle potential temperature of $T_p = 1556$ K.

To explore plume tectonics models we vary the eruption efficiency of volcanic vs. plutonic magmatism (χ_{volc}) as well as the initial composition of the upper and lower crust. The influence of rheological weakening and healing has also been studied. All models (Table 2) have the same setup as discussed in Section 2.1.1: no lithosphere initially and a crustal thickness of 35 km.

3. Results

3.1. Reference model D100b

The reference model *D100b* has a pure mafic crust. Eruption efficiency is 100% and no melt-induced weakening is considered ($\lambda_{melt} = 1$, $\dot{\varepsilon}_{healing} = 0\,s^{-1}$). From the very beginning of the model new crust is formed continuously in a heat-pipe-mode fashion (Moore and Webb, 2013), originating from the thick layer of partially molten mantle (~200 km) directly underplating the partially molten lower crust. After ~3 Myr the plume arrives and penetrates the partially molten mantle layer and the crust on top of the plume starts to thicken due to the rapid melt addition from the plume, thus creating a circular volcanic ('greenstone') area at the surface (Fig. 2a). The 'plug' of newly formed volcanic crust increases in diameter and thickness and a ring of sediments forms around it. With continuing volcanism the sediments are buried between the plug and underlying crust and the original mafic crust subsides into the mantle (Fig. 2b). At 8 Myr, eclogitisation depth of the mafic crust is reached. The unstable material drips down into the mantle as a cold high-density eclogitic drip (Fig. 2b). The downward motion of the cold crustal material into the mantle stops the upward motion of the plume, deflecting it outwards and producing new secondary plumes further away from the centre of the model. The eclogitised volcanic sequence rocks pool at the base of the model and leave narrow cylindrical partially molten traces in the partially molten upper mantle region, which become entrained in mantle convection (Fig. 2c).

After ~65 Myr of constant depletion and cooling of the uppermost mantle, the layer of partial melt has diminished to a thickness of 50–100 km and formed a depleted mantle lithosphere of a thickness of 20–40 km, with an uneven topography of the Moho and LAB. The crust is two-layered with a total thickness of 40–60 km Champion and Smithies (2007), Van Kranendonk et al. (2007, 2014). A lower layer is formed by the original mafic crust and the upper layer is comprised of the newly formed volcanic ('greenstone') sequences with bands of sediments (Fig. 2d). Eclogitised crustal drips form in several places where the crust reaches eclogitisation depth. Further model development leads to a thickening of the upper crust by continued flood volcanism and thinning of the lower crust by dripping. At this stage, crustal thinning by eclogitic drip removal occurs in phases with quiet periods in-between. During major dripping phases, drips can also initiate sheet-like delamination of the lower crust from the upper crust (often along zones weakened by sediments).

At 77 Myr a continuous layer of the lower crust starts to delaminate in a wide curved area filling the whole model domain (Fig. 2e). This large-scale delamination continues over the next 6 Myr until

Please cite this article in press as: Fischer, R., Gerya, T., Early Earth plume-lid tectonics: A high-resolution 3D numerical modelling approach. J. Geodyn. (2016), http://dx.doi.org/10.1016/j.jog.2016.03.004

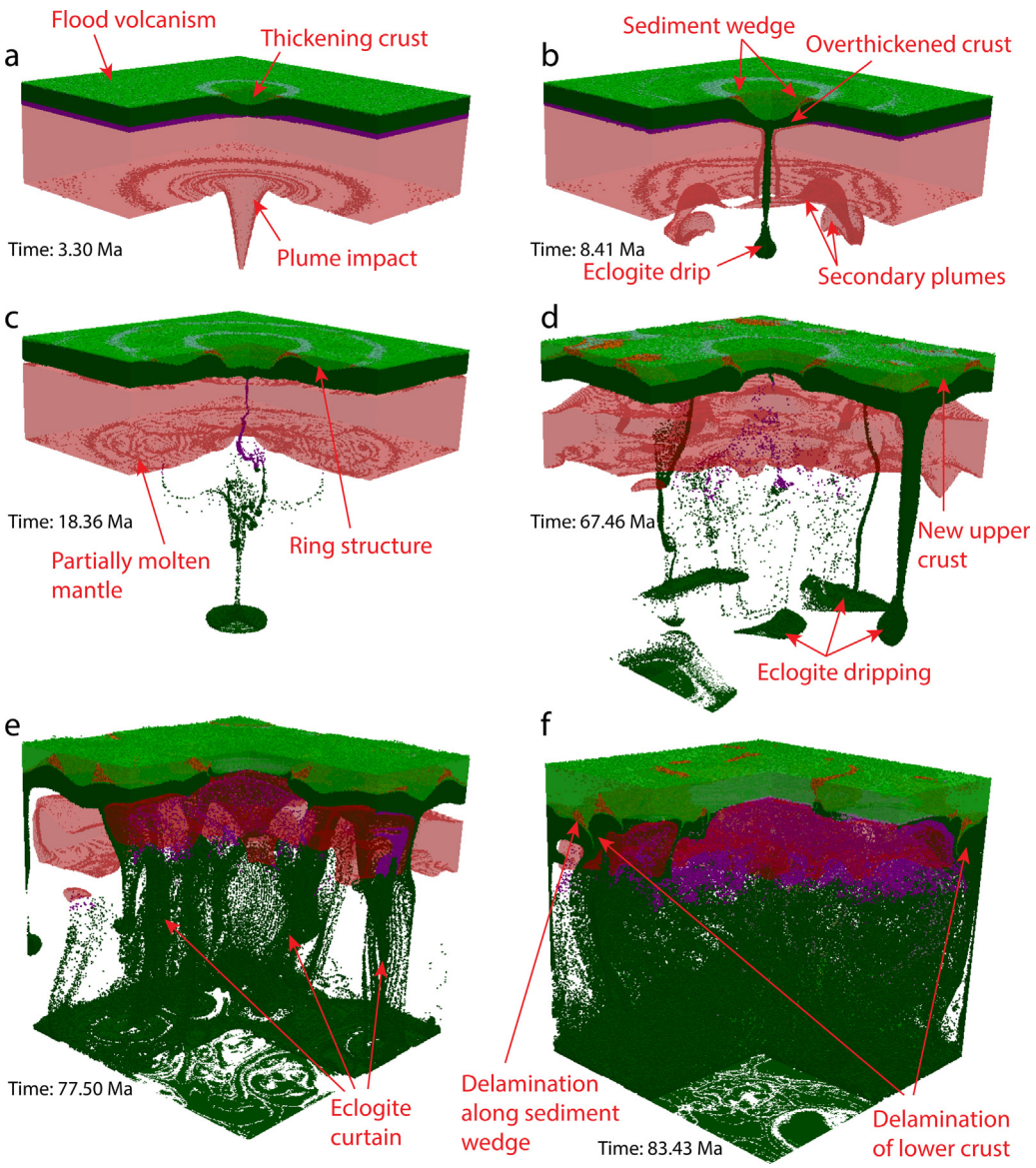

Fig. 2. Evolution of the reference model *D100b* with a pure mafic crust, eruption efficiency 100% and no melt-induced weakening ($\lambda_{melt} = 1$, $\dot{\varepsilon}_{healing} = 0\,s^{-1}$). The model shows one full cycle of crustal growth and destruction, within ~100 Myr. (a) New crust starts to form immediately, forming a thicker plug on top of the central plume. (b and c) The crust reaches eclogitisation depth and becomes thermochemically unstable. A cold eclogitic drip forms which reaches the model bottom. Secondary plumes form a ring structure in the crust. (d) Further crustal thickening leads to formation of a new upper crust and eclogite drips. (e and f) Strong dripping starts delamination of large parts of crust in a retreating sheet-like manner thereby forming an eclogite curtain.

large parts of the lower crust are removed by delamination (Fig. 2f) leaving only the upper crust consisting of newly formed volcanic rocks. The remaining crust has now a similar thickness as the original mafic crust (cf Fig. 2a and f).

3.2. *Influence of eruption efficiency* χ_{volc}

We test two different cases, one with only volcanic (model *D100b*) magmatism and one with only plutonic (model *D0b*) magmatism, to understand the influence of these two types of magmatism. A third case with present-day Earth eruption efficiency $\chi_{volc} = 20\%$ (model *D20*) is chosen for comparison. For all three cases the same initial crustal composition is chosen with a single-layered dry mafic crust.

As already described for the reference model *D100b*, pure volcanic rocks ($\chi_{volc} = 100\%$) lead to a strong growth of crust thickness (5–15 km) as well as to a two-layered crust. Both developments lead first to thinning of the lower crust by dripping and later by delamination of the lower crust in a catastrophic event which is aided by the bands of buried sediments located in the bottom of the upper volcanic crust.

Model *D0b* has an eruption efficiency $\chi_{volc} = 0$ and no melt-induced weakening ($\lambda_{melt} = 1.0$, $\dot{\varepsilon}_{healing} = 10^{-14}\,s^{-1}$). This allows us to study the case of purely plutonic magmatism. After the plume ascends through the partially molten mantle layer, a thin layer of partially molten newly formed crust builds at the bottom of the crust. This plutonic magma is positively buoyant and starts to rise through the gabbroic crust forming a diapir, which rises to a mid-crustal level of ~15 km depth (~0.5 Myr, see Fig. 3a). Within the next 5 Myr the whole lower crust is penetrated by diapirs starting from the centre of the model radially outwards (Fig. 3b). At 6 Myr a period of quiescence starts. The partially molten depleted

Please cite this article in press as: Fischer, R., Gerya, T., Early Earth plume-lid tectonics: A high-resolution 3D numerical modelling approach. J. Geodyn. (2016), http://dx.doi.org/10.1016/j.jog.2016.03.004

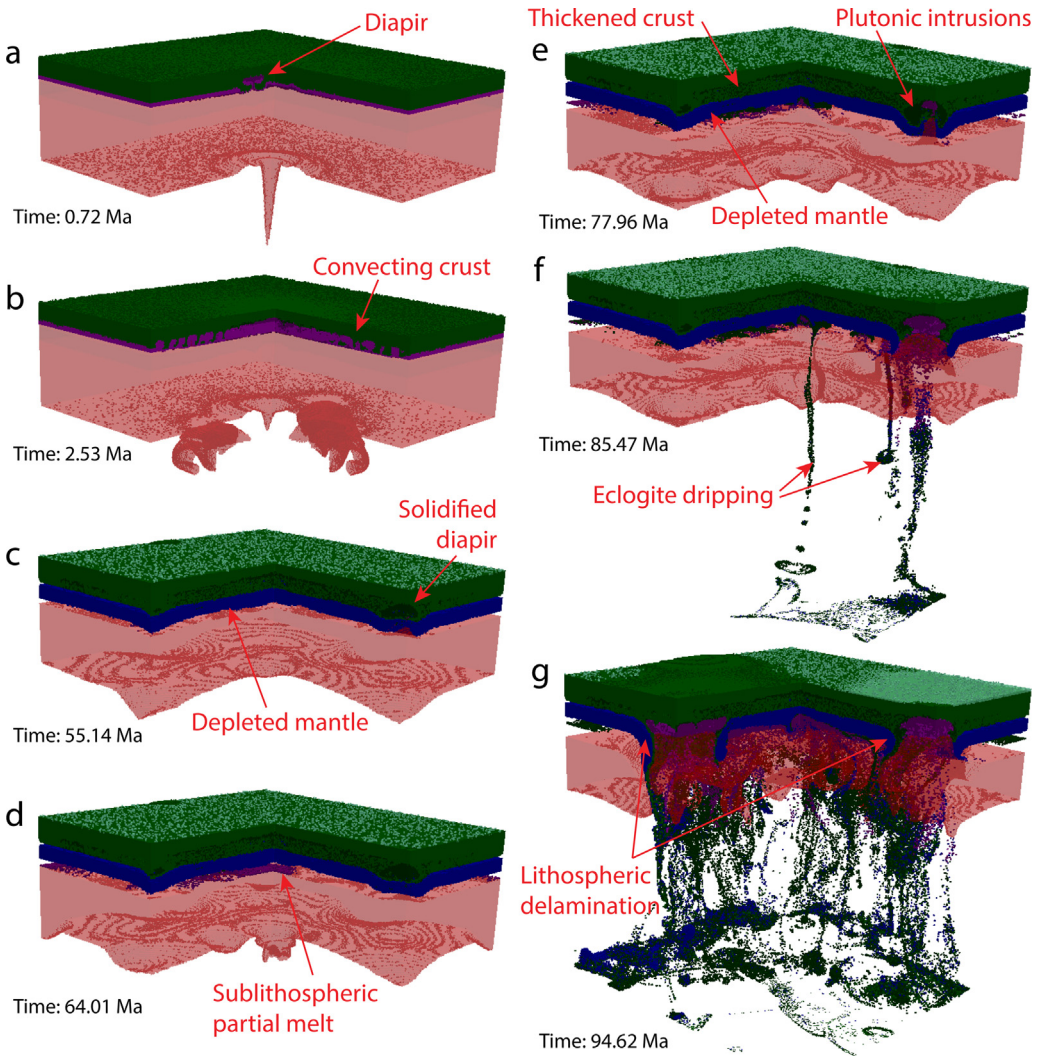

Fig. 3. Evolution of the model *D0b* with a pure mafic crust, eruption efficiency 0% (with initial emplacement of plutonic rocks at the LAB and their spontaneous propagation to the Moho) and no melt-induced weakening ($\lambda_{melt} = 1.0$, $\dot{\varepsilon}_{healing} = 2.5 \times 10^{-14}\ s^{-1}$). One full cycle of crustal growth and destruction is shown within ~100 Myr. (a and b) Accumulated partial melt at the bottom of the crust starts to rise as diapirs. (c) The rising diapirs solidify at mid-crustal level resulting in a thickened crust and mantle lithosphere. (d) Partial melt accumulates at the bottom of the lithosphere. (e) Newly accumulated partial melt starts to solidify and form eclogite or rises through the lithosphere. (f) Where crust has reached eclogitisation depth it starts to drip into the mantle. (g) Crustal diapirism and eclogite dripping causes delamination of the lithosphere and lower crust.

subcrustal mantle slowly solidifies from top to bottom within the next 20 Myr resulting in a crust of 40 km thickness underplated by a thin mantle lithosphere of 10 km.

This cycle is now repeated twice during model runtime. Between 35 and 60 Myr a second active phase can be observed with diapirs appearing and then solidifying at mid-crustal level followed by a period of quiescence. However, this activity is less strong than during the first phase. Additionally, the lithosphere is thickening from solidification of the underplating depleted partially molten mantle to a final thickness of 40 km of crust and 20 km of mantle lithosphere (Fig. 3c).

At 60 Myr a third phase of activity starts. In some regions with cold and strong lithosphere, the ascending partial melt is deposited at the bottom of the lithosphere which poses a rheological barrier for the melt propagation. The magma therefore collects at the LAB and solidifies (Fig. 3d and e). In some regions with warm and weak lithosphere the previously solidified lower crustal plutons can remelt and trigger crustal diapirism (Fig. 3e and f). These processes lead to destabilisation of the newly formed crust by eclogitisation-induced dripping (Fig. 3e and f).

In the case where magma collects at the LAB and then solidifies, the newly formed basaltic rock is transformed to high-density eclogite. It will then drip off into the mantle and remove part of the lithosphere as well. This process allows partial melt to ascend into the weakened lithosphere as diapirs that penetrate the lithosphere and ascend into the crust (Fig. 3f and g). When diapirs are able to break through the weakened lithosphere, further thickening of the crust leads to eclogitisation and dripping of the overthickened crust. The dripping initiates sheet-like delamination of the lithosphere which happens in a widening ring around the diapir centre. Together with the lithosphere the eclogitised bottom of the crust is also delaminated (Fig. 3g).

Model *D20* has a $\chi_{volc} = 20\%$ and both plutonic and volcanic magmatism is activated (Table 2 and Fig. 4). Ascending melt is transported to the surface with a 20% efficiency and accumulated at the Moho with a 80% efficiency. As in the previous model *D0b* (Fig. 3) plutonic processes are more intense in the beginning. Also, because the eruption efficiency is only 20% it takes longer for volcanic crust to grow thick enough to show the typical volcanic processes and features described for the reference model *D100b* (cf. Figs. 2 and 4).

Please cite this article in press as: Fischer, R., Gerya, T., Early Earth plume-lid tectonics: A high-resolution 3D numerical modelling approach. J. Geodyn. (2016), http://dx.doi.org/10.1016/j.jog.2016.03.004

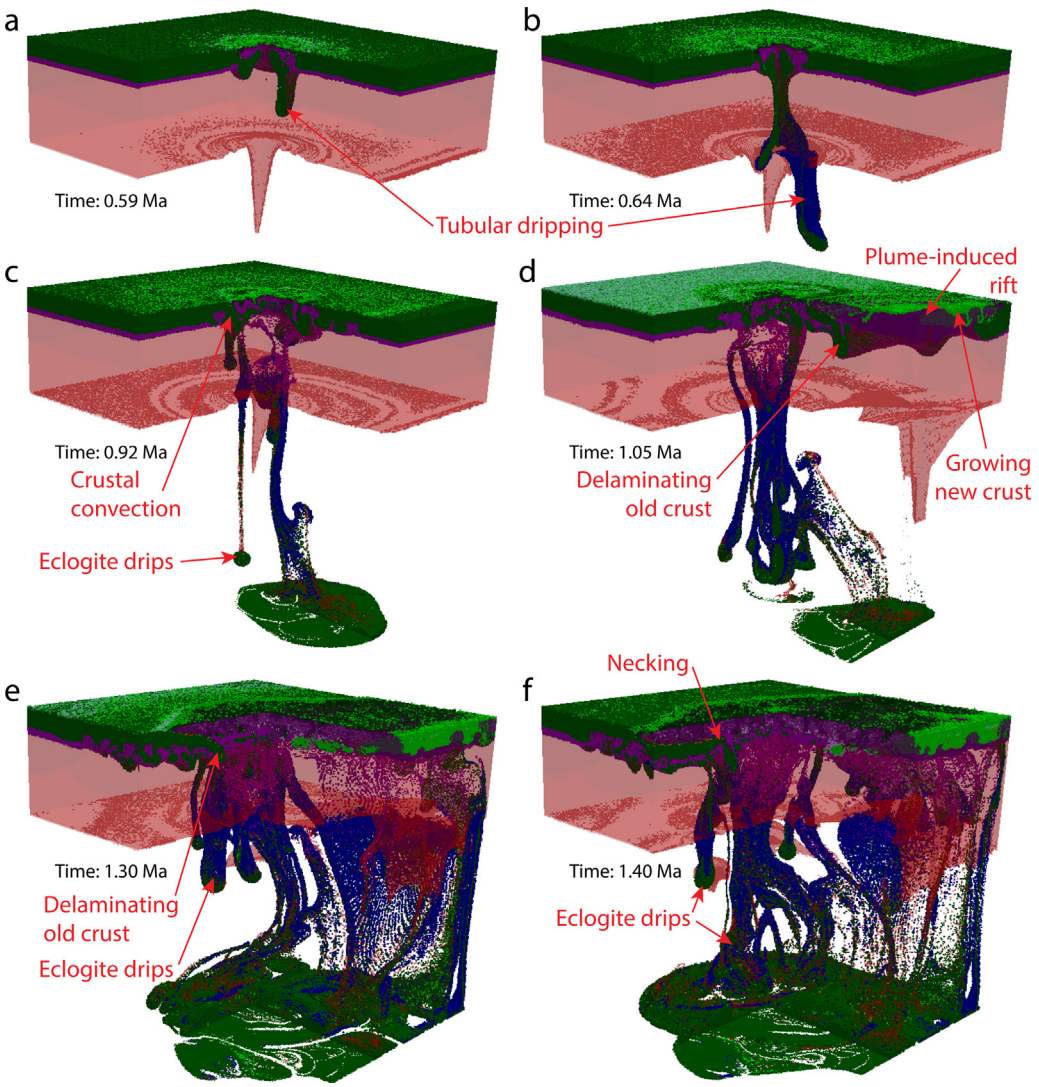

Fig. 4. Evolution of the model *D20* with a pure mafic crust, eruption efficiency 20% and melt-induced weakening ($\lambda_{melt} = 0.01$, $\dot{\varepsilon}_{healing} = 10^{-14}\,s^{-1}$). Destabilisation of the crust and the onset of an overturn event is shown. (a-b) The hot mafic melt extracted from the central plume fully penetrates the crust and starts a tubular eclogite drip. (c) Below a thin brittle lid the crust is convecting vigorously. (d) A mantle plume initiates subduction/delamination of the old crust below the newly formed lid. (e) A circular retreating subduction/ delamination of the old crust forms, assisted by eclogite drips. The slab breaks/ drips off while the lower part of the crust is still convecting.

The first 0.5 Myr are therefore characterised by pure plutonic ascent of diapirs in the crust (Fig. 4a).

Due to the activated melt-induced rheological weakening of the crust, the diapiric overturn of the crust in model *D20* happens faster than in the two end-member cases of either pure plutonic or pure volcanic magmatism (cf. Figs. 2–4). In addition, the rise of the plutonic diapirs is aided by thickening and sinking of newly formed volcanic rocks from the top. Continued diapiric uprising of the plutonic magma as well as sinking of the newly formed volcanic rocks into the crust triggers onset of crustal convection patterns concentrically broadening from the central region of the initial plume upwelling (Fig. 4c). Sinking crust then forms tubular eclogitised drips which sink into the mantle. These drips start new secondary mantle plumes which further enhance crustal convection. After 1.0 Myr a plume (close to the model boundary) is able to penetrate the crust and initiates a (semi-)circular delamination/subduction (Fig. 4d). Crustal convection still continues below the delaminating old crust which is assisted by eclogite drips and pushed downwards and forced to retreat by the spreading plume (Fig. 4e). After 1.4 Myr only a thin (few km) brittle upper crustal lid remains above the regions of the spreading plume and the sinking slab necks off and sinks into the mantle as separate eclogite drips (Fig. 4f).

3.3. Influence of felsic crust

The presence of lower-density felsic continental crust yields new tectonics and dynamics. Eruptions of basaltic magma onto felsic crust destabilise crustal layers and lead to a faster crustal overturn process. The denser newly formed mantle-derived mafic volcanic rocks sink while the positively buoyant felsic crust starts to rise. This scenario is observed in model *E100b* (eruption efficiency $\chi_{volc} = 100\%$, no melt-induced weakening $\lambda_{melt} = 1.0$ and $\dot{\varepsilon}_{healing} = 0\,s^{-1}$, see Fig. 5) which has purely felsic initial crust. In the first 3 Myr the crust on top of the plume is thickened forming a growing plug, similar to the reference model *D100b* (compare Figs. 2a and 5a). However, newly formed volcanic crust has a mafic composition and higher density than the initial crust. The thickening plug of newly formed volcanic crust therefore sinks into the initial felsic crust and after 6 Myr starts to underplate the felsic crust (Fig. 5b). Within the next 100 Myr mantle plumes in

Please cite this article in press as: Fischer, R., Gerya, T., Early Earth plume-lid tectonics: A high-resolution 3D numerical modelling approach. J. Geodyn. (2016), http://dx.doi.org/10.1016/j.jog.2016.03.004

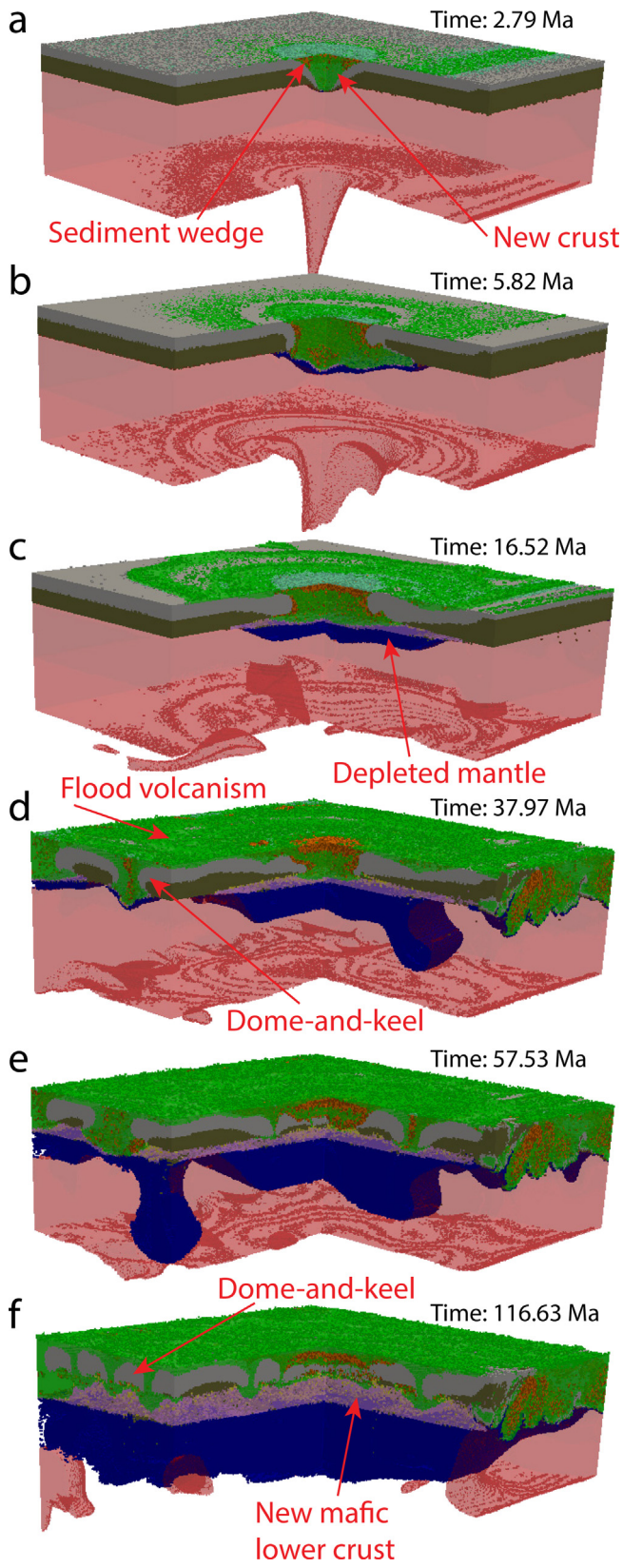

Fig. 5. Evolution of the model *E100b* with a pure felsic crust, eruption efficiency $\chi_{volc} = 100\%$ and no melt-induced weakening ($\lambda_{melt} = 1.0$, $\dot{\varepsilon}_{healing} = 0\,s^{-1}$). (a and b) Newly formed mafic crust sinks through the initial felsic crust and starts to underplate it. (c) Continuous volcanism leads to the formation of a thin lithosphere. (d and e) Doming of the initial felsic crust and sinking of the newly formed volcanic crust leads to the typical Archean dome-and-keel pattern. (f) After crustal overturn the crust consists now of a predominantly felsic upper and predominantly mafic lower layer residing on the thick mantle lithosphere.

several locations form thickening plugs of newly formed mafic crust which then sink into the underlying felsic crust and underplate it (Fig. 5c–e). After 100 Myr the surface shows large domes of upwelling felsic crust, interrupted by belts of the downwelling newly formed mafic crust which is interspersed with sediments (Fig. 5f). A new lower crustal layer of mafic composition forms from the downwelling volcanic rocks. Both upper and lower crust are heterogeneous and have highly irregular boundaries. Due to the strong magmatism the uppermost mantle becomes depleted forming a growing mantle lithosphere (Fig. 5f). The long-term crustal tectonics continue with dominantly vertical movements. There can, however, be specific situations where whole crustal blocks start to rotate and vertical movement is translated to horizontal crustal deformation.

Model *B100b* (Fig. 6) makes use of this final stable crustal layering found in model *D100b* (a lower crust of mafic composition and upper crust of felsic composition, Fig. 5f), setting it as the initial condition. All other parameters are the same as for model *E100b* ($\chi_{volc} = 100\%$, $\lambda_{melt} = 1.0$, $\dot{\varepsilon}_{healing} = 0\,s^{-1}$). Again thickening newly formed basaltic volcanic crust sinks into the felsic upper crust reaching the gabbroic lower crust. There the newly formed volcanic crust is neutrally buoyant and sinks no further. Instead it spreads along the weak upper-lower crust interface forming a new basaltic middle crust (Fig. 6a–c). After 60 Myr of thickening the crust grows to a thickness of 40–50 km residing on the lithosphere of 20–60 km (Fig. 6c). Both layers have a strongly varying topography interface depending on the state of the underlying upper-mantle convection. At this point the lower crust reaches the depth of the eclogite transition. Eclogitisation of the lower crust leads to its destabilisation and triggers cylindrical eclogitic drips sinking into the mantle (Fig. 6d). Positively buoyant material of the upper crust like sediments or felsic crust is entrained by the dripping. The downgoing tube has a core of felsic material and sediments with a mantle of eclogite enclosed by depleted lithospheric mantle (Fig. 6d). After the long period (~70 Myr) of quiescence and crustal and lithospheric growth the cold downwelling thermal-chemical inhomogeneities lead to more vigorous mantle convection and therefore more hot upwellings and more subcrustal and sublithospheric partial melting (Fig. 6e), which in turn leads to further dripping. These drips can also combine to a sheet-like downwelling which develops into a delamination of the lithosphere and lower crust (Fig. 6f). Additionally, the lithospheric/crustal lower surface is eroded by the highly vigorous mantle convection which entrains lithospheric and crustal material (Fig. 6f). 30 Myr after the beginning of the vigorous phase (100 Myr) crustal and lithospheric thickness are reduced to nearly their initial values with an upper felsic crust of 20 km and a lower mafic crust of 30 km resulting in a total crustal thickness of 50 km. At this stage, the whole mantle lithosphere is removed and the lower crust is completely replaced by the newly formed and sunken mafic volcanic rocks (Fig. 6g).

3.4. Influence of melt-induced weakening

Several models have tested the influences of the melt-induced weakening of the lithosphere (Gerya et al., 2015; Fig. 7; see Section 2.1.5 and Table 2). The local brittle/plastic strength field above a melting area is weakened during melt extraction episodes ($\lambda_{melt} = 0.01$) whereas previous strain of rocks is rapidly healed at the same time ($\dot{\varepsilon}_{healing} = 10^{-14}\,s^{-1}$). If the melt-induced weakening mechanism is suspended ($\lambda_{melt} = 1$, $\dot{\varepsilon}_{healing} = 0\,s^{-1}$) the crust remains equally strong. From similar initial conditions, models with melt-induced weakening generally develop faster (compare e.g. *D100* in Fig. 8 with melt-induced weakening and *D100b* in Fig. 2 without). Even though both models have no plutonic magmatism the small amount of crustal partial melt formed due to the initial

Please cite this article in press as: Fischer, R., Gerya, T., Early Earth plume-lid tectonics: A high-resolution 3D numerical modelling approach. J. Geodyn. (2016), http://dx.doi.org/10.1016/j.jog.2016.03.004

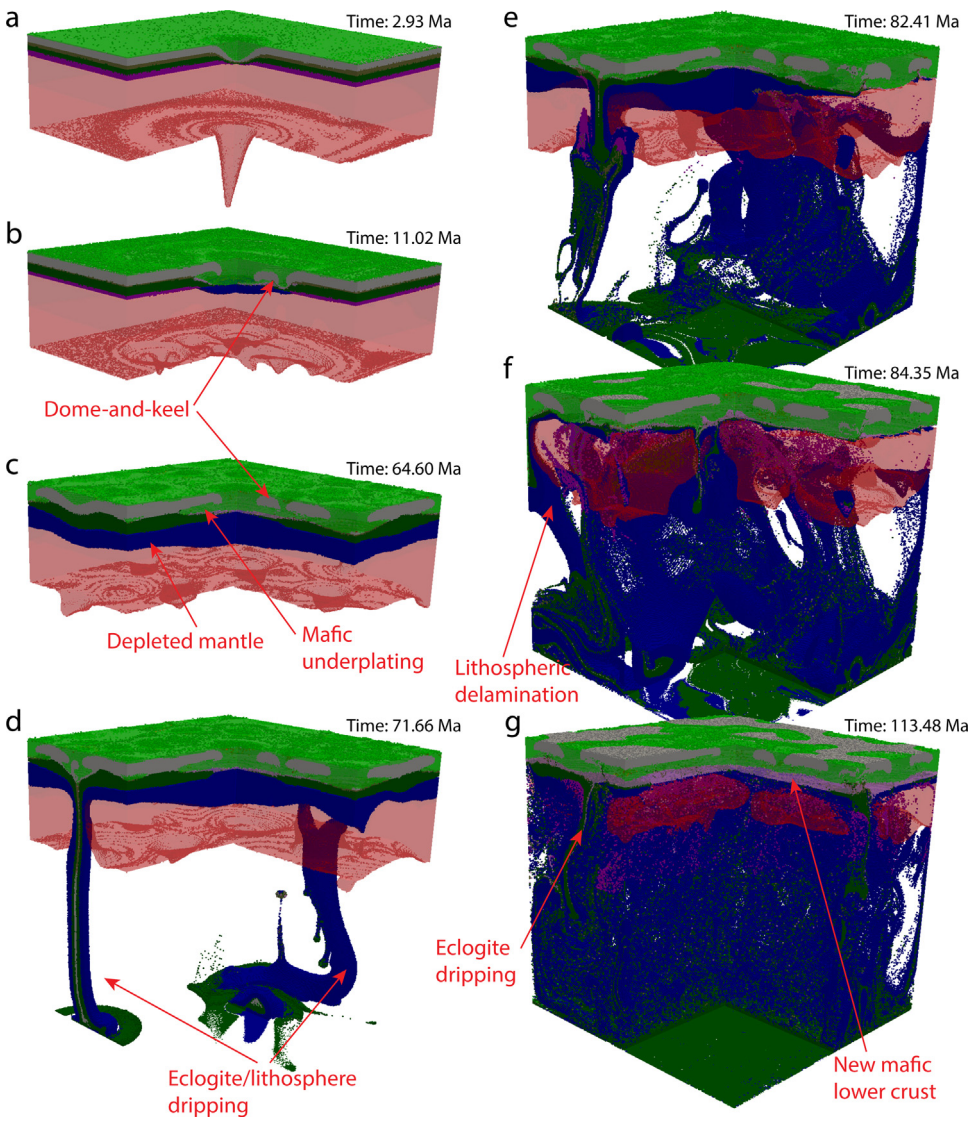

Fig. 6. Evolution of the model *B100b* with an initial upper felsic and lower mafic crust, eruption efficiency χ_{volc} = 100% and no melt-induced weakening (λ_{melt} = 1.0, $\dot{\varepsilon}_{healing}$ = $0\,s^{-1}$). (a–c) Newly formed mafic crust sinks through the felsic upper crust, forming a new mid-crustal layer. The crust is thickening to 40–50 km and a lithosphere of 20–60 km is forming. (d) The overthickened crust is dripping into the mantle forming cold tubes of eclogite and lithospheric mantle peridotite. (e–g) The dripping enhances mantle convection which leads to more subcrustal partial melting and strong removal of lithosphere and lower crust via further dripping, delamination and entrainment.

geotherm is able to rise through the crust as a diapir in the case of melt-weakened crust (Fig. 7b). Model *D100* (Fig. 8) which has the same model setup as *D100b* with pure mafic crust and eruption efficiency of χ_{volc} = 100% but with activated melt-induced weakening (λ_{melt} = 0.01, $\dot{\varepsilon}_{healing} = 10^{-14}\,s^{-1}$) shows a similar model development to model *D100b* (Fig. 2). In both models the crust starts to thicken above the rising mantle plume. A plug of newly formed volcanic crust is forming and as the crust reaches eclogitisation depth, eclogite drips off as a cold thermal–chemical instability (Fig. 8a). This process takes ~8 Myr without melt-weakening. In the case of melt-induced weakening the whole process only takes ~1 Myr as the weakened crust percolated by melts is not able to support as much weight and the growing plug of newly formed volcanic crust can more easily sink into the initial crust. In addition, partially molten lower crust (which forms due to the steep crustal geotherm) rises through the weakened middle crust in form of diapirs (Fig. 7b). After 3 Myr the strong weakening of the crust and the rising lower crustal diapirs lead to crustal convection. In regions of newly formed downwelling crust the crust can locally grow very thick and reach eclogitisation depth. Eclogite dripping due to overthickening therefore occurs early in model development (3 Myr, see Fig. 8b) whereas the same eclogite drips in model *D100b* without melt-induced weakening only occur after 60 Myr (Fig. 2d).

3.5. Influence of layered crust

In the following, three models with a dual-layer crust are introduced, with an upper crust of wet quartzite and a lower crust of plagioclase An_{75} rheology. All three models have an eruption efficiency of χ_{volc} = 20% and melt-induced weakening (λ_{melt} = 0.01, $\dot{\varepsilon}_{healing} = 10^{-14}\,s^{-1}$).

Model *C20* (Fig. 9) contains a layered crust of upper hydrated mafic crust and lower dry mafic crust. In this type of model an intracrustal layer of partially molten upper crust as well as a deep layer of partially molten lower crust is formed. Accumulated

Please cite this article in press as: Fischer, R., Gerya, T., Early Earth plume-lid tectonics: A high-resolution 3D numerical modelling approach. J. Geodyn. (2016), http://dx.doi.org/10.1016/j.jog.2016.03.004

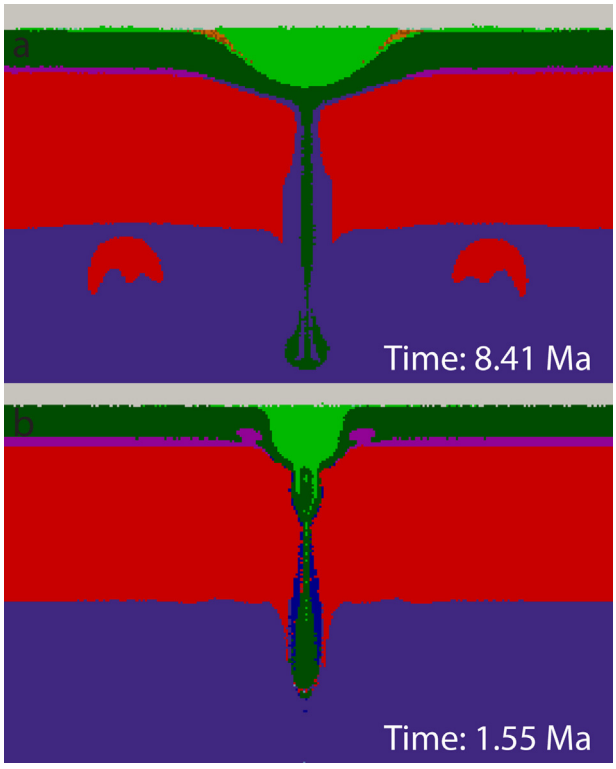

Fig. 7. Comparison between models (a) *D100b* without melt-induced weakening ($\lambda_{melt} = 1.0$, $\dot{\varepsilon}_{healing} = 0\,s^{-1}$) and (b) *D100* with melt-induced weakening ($\lambda_{melt} = 0.01$, $\dot{\varepsilon}_{healing} = 10^{-14}\,s^{-1}$). Both models have the same initial composition of pure mafic crust and an eruption efficiency of $\chi_{volc} = 100\%$. Both panels show a 2D slice at the time of the first eclogite drips. Model development is similar but in the case of (b) melt-induced weakening it is much faster and more localised. Due to the weakened crust, partial melt is able to rise as diapirs in the lower crust.

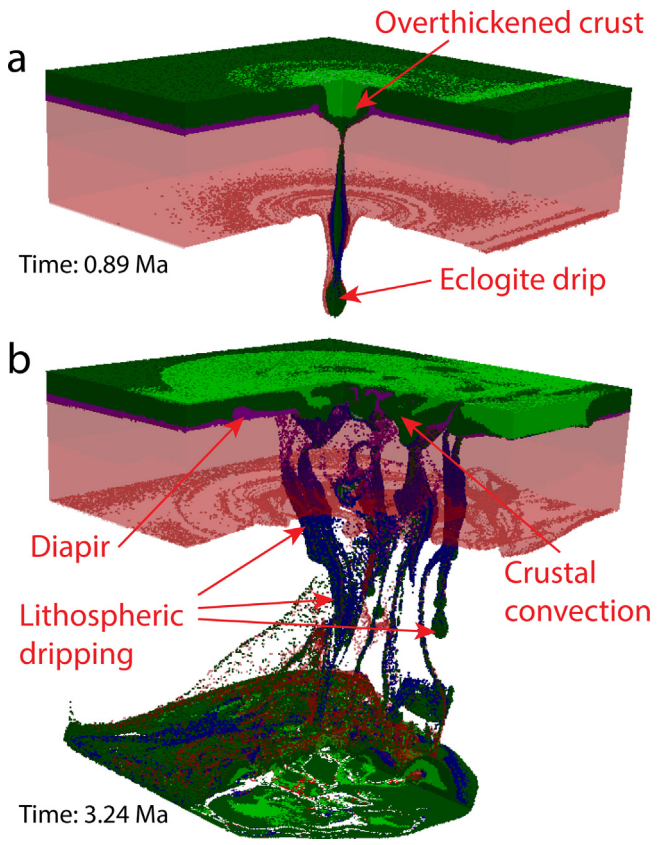

Fig. 8. Evolution of the model *D100* with initial composition of pure mafic crust, $\chi_{volc} = 100\%$ and melt-induced weakening ($\lambda_{melt} = 0.01$, $\dot{\varepsilon}_{healing} = 10^{-14}\,s^{-1}$). (a) Earliest model development is similar to model *D100b* (Fig. 2) but with clear signs of weakening. (b) Weakening of the crust leads to crustal convection and local overthickening which causes formation of eclogite drips.

partial melt can easily rise from the Moho through the melt-weakened lower crust and reach the midcrustal partial melt layer. The midcrustal layer destabilises as well and the diapir can reach the surface (Fig. 9a and b). The initial large diapir on top of the mantle plumes leads to partial melt spreading on top of the crust. The surface of the diapir is solidified while its edges are compressing the crust, pushing it downwards (Fig. 9a). The thickening is also aided by newly formed volcanic crust. The thickened crust along the edges of the diapir forms eclogite and drips off into the mantle in a open tube shape (Fig. 9a). These drips initiate further plumes which rise in a concentric pattern around the initial central plume, forming a ring of rising diapirs in the crust. Both processes happen in rapid succession forming a striking pattern of outward growing rings comprised of alternating diapirs and eclogite drips (Fig. 9b). Due to the continuous strong magmatic activity the partial melt layer is strongly depleted but no solid lithosphere is formed. Cold eclogite drips lead to freezing of the depleted hot mantle and the formation of a solid carapace of lithospheric mantle peridotite around the sinking drips (Fig. 9b–d). Further model development leads to a complete mixing of the crust resulting in a thin brittle crustal lid (~10 km) above the lower partially molten layer (~30 km) which is vigorously convecting (Fig. 9c and d). Both layers are strongly inhomogeneous with laterally varying topography of their upper and lower boundaries.

Model *A20* has a purely felsic crust. It is two-layered with an upper crust with wet quartzite rheology and a lower crust with plagioclase An_{75} flow law. On top of the rising mantle plume at the bottom of the crust enough partial melt is accumulated to be able to rise through the entire crust (Fig. 10a). New magmatic crust is formed on top of this molten diapir and starts to sink along its edges. This downward motion triggers an upward motion further away from the model centre and with it a second ring of diapirs (Fig. 10a and b). As in the model *C20* described above both crustal layers are partially molten at the bottom. Moving outwards from the central disturbance diapirs start to rise from the upper and lower layer of partial melt independently leading to a separate overturn of upper and lower crust (Fig. 10b and c). However, after ~1 Myr the two separately convecting layers start to mix (Fig. 10d), soon (~3 Myr) forming an upper solid layer and a lower partially molten layer (Fig. 10d and e). However, the crust is still strongly convecting with upwelling partial melt and sinking solid upper crust. Above regions of hot mantle upwellings corresponding to the original and secondary plumes, the initial upper crustal layer is destroyed by rising diapirs and new basaltic crust is formed (Fig. 10c and f). This newly formed crust sinks through the solid and partially molten felsic crust to the Moho and leaves only thin belts of mafic traces at the surface (Fig. 10g) comparable with models *B100b* (Fig. 6) and *E100b* (Fig. 5). In regions of cold mantle downwellings depleted partially molten upper mantle solidifies and forms embryonic dripping mantle lithosphere (Fig. 10f–h).

Model *B20* (Fig. 11) has the same setup as *C20* (Fig. 9) and *A20* (Fig. 10) but with a hydrated felsic upper crust and a mafic lower crust. The central crustal diapir formed on top of the mantle plume is able to rise through both crustal layers. New mafic crust is formed around the edges of the diapir and a ring of secondary diapirs are initiated at the bottom of the lower crust (Fig. 11a). The partial melt layers of upper and lower crust start to rise separately and upper and lower crust start to overturn individually (Fig. 11b and

Please cite this article in press as: Fischer, R., Gerya, T., Early Earth plume-lid tectonics: A high-resolution 3D numerical modelling approach. J. Geodyn. (2016), http://dx.doi.org/10.1016/j.jog.2016.03.004

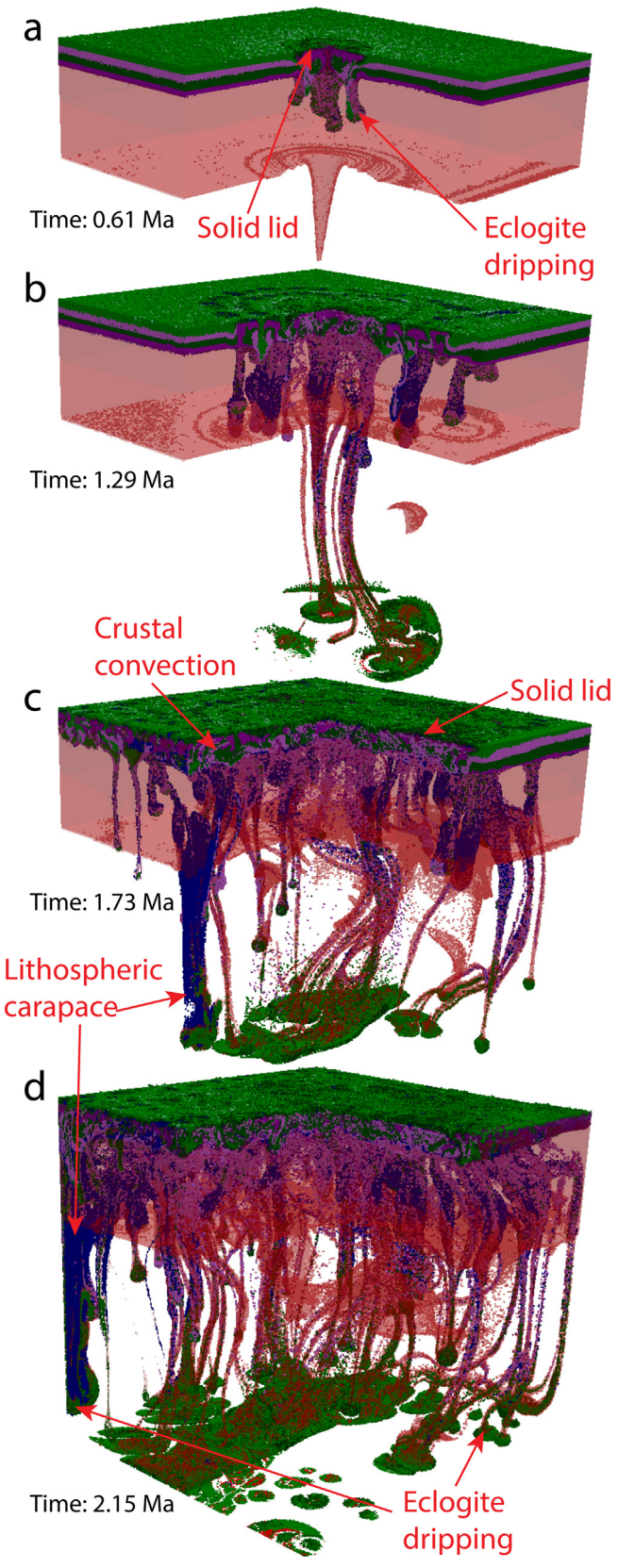

Fig. 9. Evolution of the model *C20* with an upper hydrated mafic crust and a lower dry mafic crust. The eruption efficiency is χ_{volc} = 20% and melt-induced weakening is activated (λ_{melt} = 0.01, $\dot{\varepsilon}_{healing} = 10^{-14}\,s^{-1}$). (a) The melt-weakened crust allows diapirs to rise through the crust to the surface. Thickening of the crust around the rising diapir due to compression and newly formed volcanic crust leads to eclogitisation and tube-shaped drip off. (b) Dripping initiates further diapirs which rise in a concentric pattern around the initial central plume, which together with further drips form a pattern of outward growing rings comprised of alternating diapirs and eclogite drips. (c and d) Complete mixing of the crust leads to a thin brittle lid on top of the vigorously convecting crust.

c). Rising mantle plumes are able to produces enough magma such that large diapirs on top of the plumes can reach the surface. New mafic crust is produced at the surface (Fig. 11d), which has negative buoyancy compared to the underlying felsic crust and starts to subside as soon as plume activity ceases (Fig. 11e). This newly formed volcanic crust can only sink through the upper felsic layer and accumulates at midcrustal level leaving behind thin belts of mafic material at the surface (Fig. 6f). After 20 Myr of model development the large-scale crustal structure becomes rather similar to the initial condition for this experiment: 20 km of felsic upper crust and 20 km of mafic lower crust. Further model development leads to the formation of embryonic mantle lithosphere in places of mantle downwellings. After 26 Myr the lower crust reaches the eclogite transition depth and eclogitised mafic crust drips into the mantle.

4. Discussion

4.1. Magmatic processes, short-term crustal thickening and over-turn, crustal tectonics

Due to the higher temperature in the early Earth, all magmatic processes are intensified. Strong volcanism is produced by heat-piping (Moore and Webb, 2013) and deposited at the surface in large volumes of high-temperature lava-flows similar to present-day flood basalts. This flood volcanism was common in the Archean (Arndt, 1999; Van Kranendonk et al., 2007, 2014). If it occurs on top of mafic crust (models D and C20), the crust is thickened by adding newly formed volcanic rocks on the top (Smithies et al., 2009; Van Kranendonk et al., 2004, 2014). If this flood volcanism occurs on felsic crust an unstable layering is established, which creates favourable conditions for gravitational overturns (Collins et al., 1998; Champion and Smithies, 2007; Van Kranendonk et al., 2004, 2014a, 2014).

At the same time, magmatic intrusions are accumulated in the lower crust and (sometimes) below the thin mantle lithosphere (Fig. 3), which triggers crustal diapirism developing in several phases.

Both processes – flood volcanism on felsic crust, as well as plutonic magmatism – encourage convective overturn of the crust. In a stronger crust, sinking of mafic newly formed volcanic rocks into the felsic crust and diapiric rise of the underlying felsic crust leads to a convective overturn and the formation of the typical dome-and-keel pattern observed in several cratons, e.g. East Pilbara in Western Australia (Van Kranendonk et al., 2004; Hickman, 2004), Kaapvaal in South Africa (Van Kranendonk, 2011a). In a weaker crust, where a larger part of the crust is partially molten, this diapiric sinking and rising takes on the form of a rapid intense convection, driven by the sinking of cold basaltic crust and the rising of hot plutonic partially molten rocks (Fig. 12a; Collins et al., 1998).

In addition, burial of radiogenic felsic crust under mafic volcanic rocks may have an important effect for creating a hotter crustal geotherm (Gerya et al., 2002; Rey et al., 2003; Sandiford et al., 2004). It is, however, difficult to evaluate this effect for studied models due to the dominance of heat advection processes by crustal overturns.

The mafic newly formed volcanic rocks sink through the felsic crust and accumulate at its bottom, thus effectively forming a new lower crust. If a lower mafic crust is already present, the sinking material is added at the upper to lower crustal interface, in this way

Please cite this article in press as: Fischer, R., Gerya, T., Early Earth plume-lid tectonics: A high-resolution 3D numerical modelling approach. J. Geodyn. (2016), http://dx.doi.org/10.1016/j.jog.2016.03.004

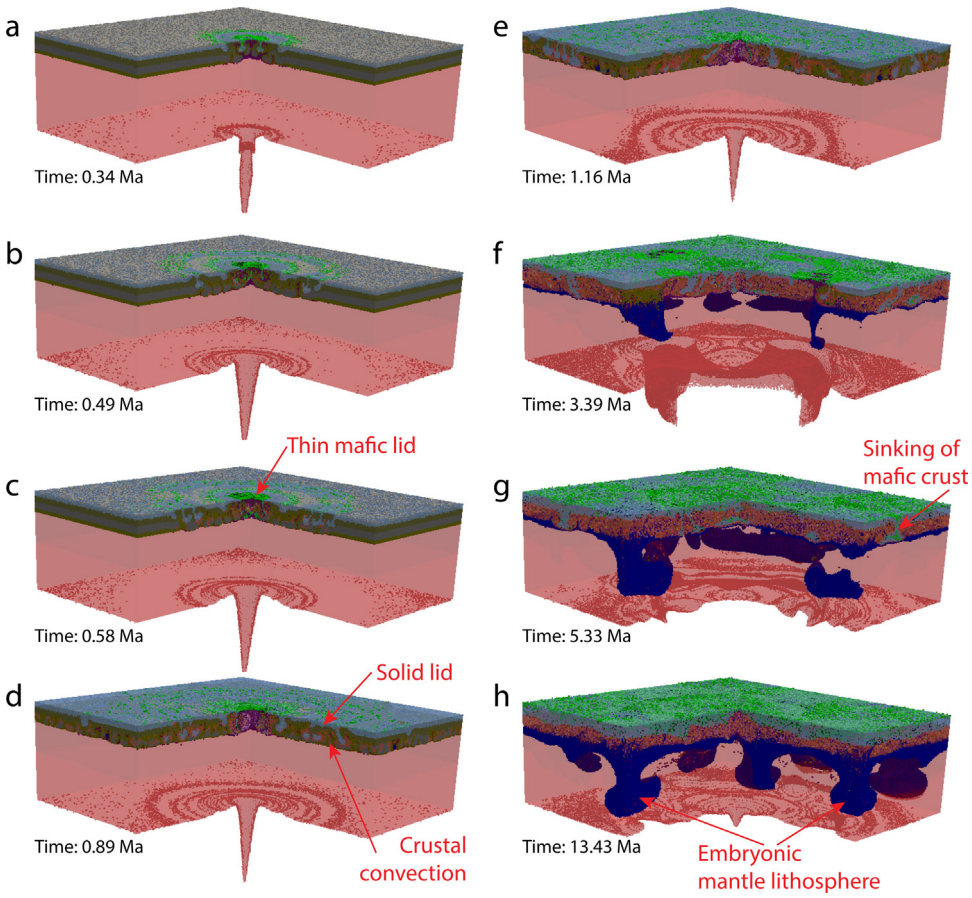

Fig. 10. Evolution of the model *A20* with an upper hydrated and a lower dry felsic crust. The eruption efficiency is χ_{volc} = 20% and melt-induced weakening is activated (λ_{melt} = 0.01, $\dot{\varepsilon}_{healing} = 10^{-14}$ s^{-1}). (a) The melt-weakened crust allows diapirs to rise through the crust to the surface. (b and c) Thickening of the crust around the rising diapir due to compression and newly formed volcanic crust leads to separate convection in the upper and lower crust. (d and e) Formation of a thin brittle upper lid introduces the whole-crustal convection regime. (f) On top of mantle plumes the original crust is destroyed and a thin new mafic crust is formed. (g and h) The newly formed mafic crust sinks through the entire crust leaving only thin traces at the surface.

thickening the lower crust. A similar structure has been observed for both the Pilbara and the Kaapvaal craton (Van Kranendonk et al., 2014).

4.2. Crustal thickening, destabilisation and recycling into the mantle

As described above the crust is thickening over time in several ways due to intense magmatism. Due to crustal convective overturn the lower crust has in most cases mafic composition. As soon as the thickening crust reaches eclogite PT-conditions the mafic lower crust transforms to eclogite and drips off into the mantle. These thermochemical instability of negatively buoyant material can trigger further instabilities of thermal and thermochemical nature leading to dripping of the mantle lithosphere and eclogitised lower crust, which may also incorporate felsic crustal rocks (Fig. 6d). Drips can have several forms: cylindrical triggered by overthickening, hollow cylindrical curtains e.g. triggered by plume (Gerya et al., 2015) and linear (sheet-like) curtains triggered by horizontal compression (Gögüs and Pysklywec, 2008a; Fischer and Gerya, submitted for publication). Convective mantle return flow due to dripping (Gögüs and Pysklywec, 2008b) can lead to weakening of the lithosphere and lower crust and start delamination along a weak zone (Gögüs and Pysklywec, 2008a) like the Moho, the lower-upper crust boundary or even a middle crustal weak buried (meta)sedimentary layer (Fig. 2e and f).

4.3. Long-term tectonic processes

From a long-term view (10–100 s of Myr) the short-term event of crustal overturn as described above happens several times in succession as short singular events. During several overturn events the crust is thickening during the period of relative quiescence ('growth phase') until the lower crust becomes gravitationally unstable due to its thickening and eclogitisation A short turbulent chaotic 'removal phase' follows with delamination of large parts of the lower crust and mantle lithosphere within a few Myr: a resurfacing event. After this resurfacing event thickness of the crust changes to its original (equilibrium) value whereas mantle lithosphere is completely removed and starts to grow again from the depleted hot upper mantle (Figs. 2, 3 and 6). Similar processes can also be observed in nature where Hickman and Van Kranendonk (2004) documented in the East Pilbara several active volcanic cycles of ~15 Ma interrupted by long periods quiescence.

4.4. Mantle convection patterns and lithospheric growth

The mantle in all models is vigorously convecting. In most models a two-layered mantle convection can be observed. The partially molten part of the mantle has a thickness of ~120 km. It is forming a separate layer (marked in red in Fig. 12a and b) which is convecting in a strongly unstable, chaotic manner, forming several small-scale convection cells, which are strongly influenced

Please cite this article in press as: Fischer, R., Gerya, T., Early Earth plume-lid tectonics: A high-resolution 3D numerical modelling approach. J. Geodyn. (2016), http://dx.doi.org/10.1016/j.jog.2016.03.004

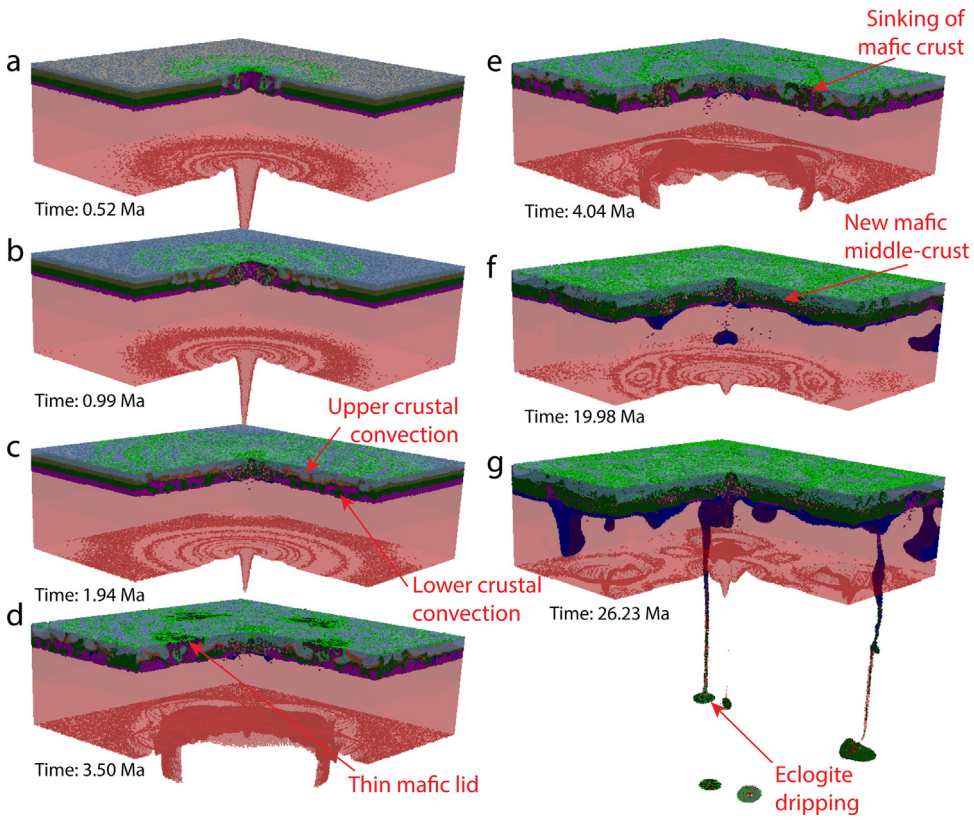

Fig. 11. Evolution of the model *B20* with an upper hydrated felsic crust and a lower dry mafic crust. The eruption efficiency is χ_{volc} = 20% and melt-induced weakening is activated (λ_{melt} = 0.01, $\dot{\varepsilon}_{healing} = 10^{-14}$ s^{-1}). (a) Diapirs rise through the melt-weakened crust to the surface. (b-c) The rising central diapir initiates separate upper and lower crustal convection. (d) On top of mantle plumes the original crust is destroyed and a thin new mafic crust is formed. (e and f) The newly formed mafic crust sinks to the upper-lower crust boundary forming a new mafic middle crust. (g) Eclogite drips sink from the overthickened lower mafic crust into the mantle.

by rising plumes from below as well as cold sinking eclogitised crustal material from above (Fig. 12a). The lower part of the model forms a second convection layer with more stable, larger-scale convection cells below the partially molten mantle layer. During crustal and lithospheric growth 1–2 stable convection cells can be observed. However, also in this more stable layer the convection patterns change several times during the model run, either due to plumes rising from different location at the bottom boundary or due to cold crustal and lithospheric material sinking down into the mantle.

4.5. PT-conditions for generation of TTG-crust

The timing, volume and detailed process of the formation of felsic continental crust are strongly debatable. However, most authors agree that felsic crust and with it its early Earth representation, the TTG rocks, must have formed by successive remelting of hydrated mafic rocks (Hawkesworth and Kemp, 2006). Even though this code does not support formation of felsic rocks from basaltic partial melt, it is still possible to evaluate the PT-conditions for occurrence of partially molten mafic rocks, which would potentially act as the source melt regions for the formation of TTGs. According to Moyen (2011) approximately 20% of all TTGs stem from sources at low pressure (0–10 kbar), 60% stem from medium pressure sources of 10–20 kbar and another 20% from high-pressure sources >20 kbar.

Taking into account all basaltic partial melt and calculating their percentage for low-, mid- and high-pressure range for two different models *C20* (Fig. 13a) and *D100b* (Fig. 13b), however, leads to very different results. Even though both models start out with the same model setup of 35 km of mafic crust, model *D100b* at 83 Myr ends up with nearly no partially molten basaltic crust in the low-pressure region, 30% in the mid-pressure region and 70% in the high-pressure region (Fig. 13b). Whereas in the case of model *C20* (at 2.7 Myr) the partially molten basaltic crust is distributed as follows: 70% in the low-pressure, 20% in the mid-pressure and 10% in the high-pressure region (Fig. 13a).

The last available timestep of model *C20* is much younger than model *D100b*. Model *C20* can therefore be interpreted to represent a very early stage of evolution of model *D100b*. This early first stage which is dominated by crustal overturn and convection mainly produces partially molten basalt in the uppermost region between 0 and 10 kbar (Fig. 13a). In Fig. 13b from model *D100b* crustal overturn and a catastrophic resurfacing event has already occurred and the model is back in its initial stage where the crust starts to thicken again. In this case nearly no partial melt is found in the crust but the major regions of basalt melting are located within deep eclogitised domains. These regions correspond either to partially molten lower crust or to partially molten remnants of dripping or delaminating crust. The total volume of partially molten basaltic rocks in *D100b* is only 15% of their volume present in *C20*. The volume of mid- and high-pressure partially molten basaltic crust is about the same, while the volume of low-pressure partially molten basaltic crust in model *C20* is nearly 1000 times higher.

We, therefore, conclude that the amount of low-, mid- and high-pressure basaltic TTG source melt varies throughout the different stages of the Archean tectonic process and major TTG-crust formation episodes should correspond to short, hot and rapid overturn events ('removal phase', Figs. 3b and 12a) rather than to periods of relative tectono-magmatic quiescence and lithospheric thickening ('growth phase', Figs. 3e and 12b, see also Smithies et al. (2009)).

Please cite this article in press as: Fischer, R., Gerya, T., Early Earth plume-lid tectonics: A high-resolution 3D numerical modelling approach. J. Geodyn. (2016), http://dx.doi.org/10.1016/j.jog.2016.03.004

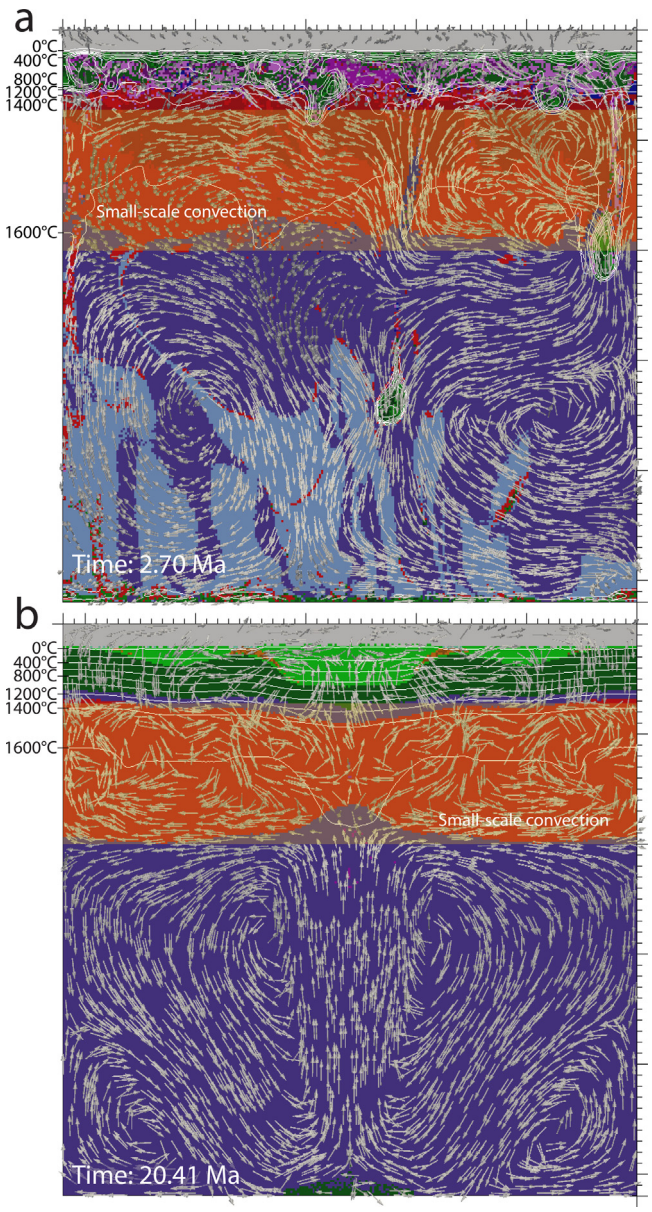

Fig. 12. 2D compositional slice of (a) model *C20* (Table 2 and Fig. 9) and (b) model *D100b* (Table 2 and Fig. 2). Position of the slice is given in Fig. 1a. White isolines mark the temperature, arrows mark the velocity field. Three distinct convective layers can be observed: (1) a lower stably convecting mantle layer, (2) an upper chaotically convecting mantle layer (marked in red) and (3) the convecting crust.

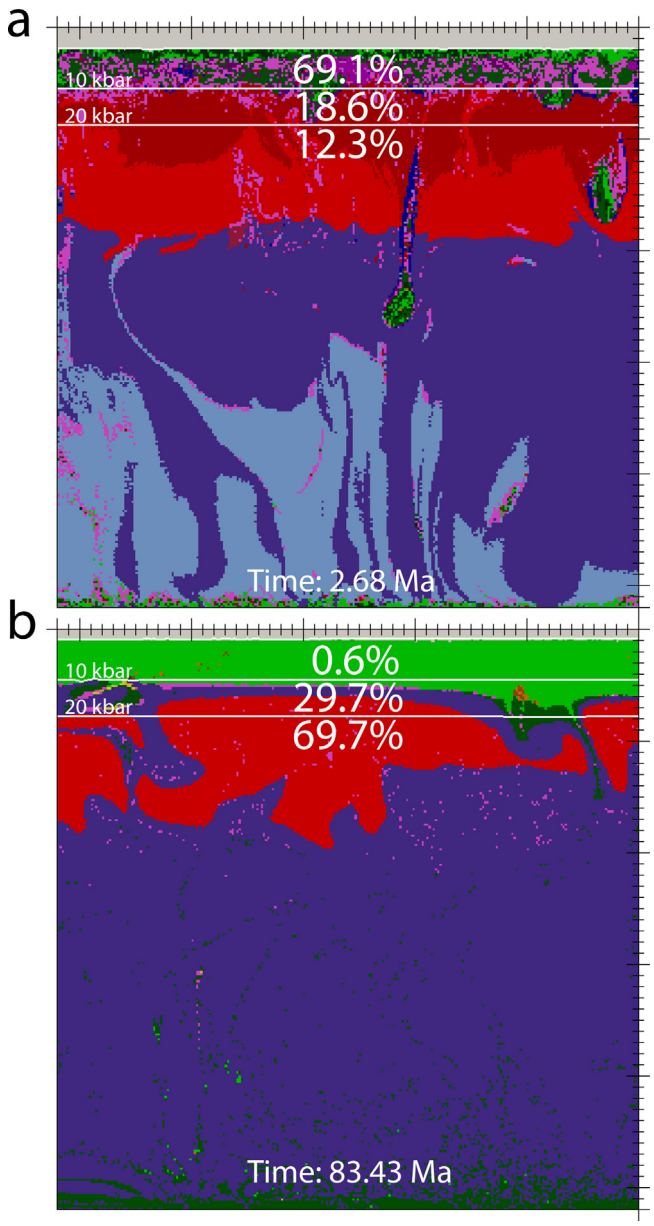

Fig. 13. 2D compositional slice of (a) model *C20* (Table 2 and Fig. 9) and (b) model *D100b* (Table 2 and Fig. 2). Position of the slice is given in Fig. 1a. White isolines mark the 0, 10 and 20 kbar pressure isosurface. All hydrated partially molten mafic rocks, which act as potential TTG source melts, are marked in purple and their percentage in each pressure band is given.

4.6. Consequences for subduction initiation

The shift from early Earth plume-lid tectonics to plate tectonics is one of the big research questions (Shirey and Richardson, 2011; Van Kranendonk, 2011b; Gerya et al., 2015, and references therein). A possible answer would be plume induced subduction (Ueda et al., 2008; Van Kranendonk, 2010; Gerya et al., 2015). Similar beginnings are observed in several models (mainly with melt induced weakening): e.g. Figs. 2e and f, 3f and g, 4d–f and 9a. However, the sinking tube-shaped 'slab' is much too weak (see also van Hunen and van den Berg, 2008) to continue a subduction and rather forms a circular drip and necks off while the crustal plateau continues to grow as described by (Champion and Smithies, 2007; Van Kranendonk et al., 2007, 2014; Gerya et al., 2015).

5. Conclusion

Archean plume-lid tectonics are predominantly tectono-magmatic and mainly driven by strong crustal and lithospheric growth. The overthickened unstable crust is removed by means of eclogite drips or drip tectonics (Herzberg, 2014) and delamination. Asthenospheric mantle flow on one hand drives crustal growth, deformation and episodic thinning by eclogite recycling and on the other hand is strongly modified by dripping of crustal material back into the mantle. We also found that the crust forms a separate convection layer, with convection assisted by doming of magmatic plutons and sinking of basaltic crust formed by flood volcanism (Arndt, 1999; Van Kranendonk, 2011a). This yields an extremely efficient way of heat removal through the crust via convection and conduction through the thinned brittle upper crustal lid and could

Please cite this article in press as: Fischer, R., Gerya, T., Early Earth plume-lid tectonics: A high-resolution 3D numerical modelling approach. J. Geodyn. (2016), http://dx.doi.org/10.1016/j.jog.2016.03.004

provide an answer to the Archean paradox as described by Moresi (2013) in addition to the heat-pipe model (Moore and Webb, 2013). Furthermore we found Archean plume-lid tectonics to be separated into two distinct phases: (1) A longer and relatively quiet 'growth phase', where crust and lithosphere grow in thickness. (2) This is followed by a short and catastrophic 'removal phase', where unstable parts of the crust and lithosphere are removed first via dripping and later via delamination. This pattern of episodic overturn has already been suggested for the Archean by several authors: Kröner and Layer (1992), Zegers and van Keken (2001), van Thienen et al. (2005b), Bédard (2006).

Acknowledgements

This study was co-funded by an ETH-grant ETH-37_11-2, by an ERC ITN-grant ZIP (T.G.), by a SNF-project Swiss-AlpArray (T.G.), by a SNF-grant 200021_149252. Simulations were performed on the ETH-Zurich Brutus and Euler clusters. Constructive reviews of Martin Van Kranendonk and an anonymous reviewer are appreciated. Daniel Bower is thanked for proofreading of the manuscript.

Appendix A. Supplementary data

Supplementary data associated with this article can be found, in the online version, at http://dx.doi.org/10.1016/j.jog.2016.03.004.

References

Armann, M., Tackley, P.J., 2012. Simulating the thermochemical magmatic and tectonic evolution of Venus's mantle and lithosphere: two-dimensional models. J. Geophys. Res. Planets 117, E12003.
Arndt, N., 1999. Why was flood volcanism on submerged continental platforms so common in the Precambrian? Precambrian Res. 97 (3–4), 155–164.
Bédard, J.H., 2006. A catalytic delamination-driven model for coupled genesis of Archaean crust and sub-continental lithospheric mantle. Geochim. Cosmochim. Acta 70 (5), 1188–1214.
Benn, K., Mareschal, J.-C., Condie, K.C., 2006. Introduction: Archean geodynamics and environments. In: Archean Geodynamics and Environments. American Geophysical Union, pp. 1–5.
Bittner, D., Schmeling, H., 1995. Numerical modelling of melting processes and induced diapirism in the lower crust. Geophys. J. Int. 123 (1), 59–70.
Breuer, D., Moore, W.B., 2007. Dynamics and thermal history of the terrestrial planets, the Moon, and Io. In: Gerald, S. (Ed.), Treatise on Geophysics. Elsevier, Amsterdam, pp. 299–348.
Brown, M., 2007. Metamorphic conditions in orogenic belts: a record of secular change. Int. Geol. Rev. 49 (3), 193–234.
Burov, E., Gerya, T., 2014. Asymmetric three-dimensional topography over mantle plumes. Nature 513 (7516), 85–89.
Champion, D.C., Smithies, R.H., 2007. Chapter 4.3. Geochemistry of Paleoarchean granites of the East Pilbara Terrane, Pilbara Craton, Western Australia: implications for early Archean crustal growth. In: Martin, J., van Kranendonk, R.H.S., Vickie, C.B. (Eds.), In: Developments in Precambrian Geology, vol. 15. Elsevier, pp. 369–409.
Clauser, C., Huenges, E., 1995. Thermal conductivity of rocks and minerals. In: Ahrens, T. (Ed.), In: Rock Physics and Phase Relations, vol. 3. AGU Reference Shelf, pp. 105–126.
Collins, W., Van Kranendonk, M.J., Teyssier, C., 1998. Partial convective overturn of Archaean crust in the east Pilbara Craton, Western Australia: driving mechanisms and tectonic implications. J. Struct. Geol. 20 (9), 1405–1424.
Connolly, J.A.D., 2005. Computation of phase equilibria by linear programming: a tool for geodynamic modeling and its application to subduction zone decarbonation. Earth Planet. Sci. Lett. 236 (1–2), 524–541.
Crameri, F., Schmeling, H., Golabek, G.J., Duretz, T., Orendt, R., Buiter, S.J.H., May, D.A., Kaus, B.J.P., Gerya, T.V., Tackley, P.J., 2012. A comparison of numerical surface topography calculations in geodynamic modelling: an evaluation of the sticky air' method. Geophys. J. Int. 189 (1), 38–54.
Crisp, J.A., 1984. Rates of magma emplacement and volcanic output. J. Volcanol. Geotherm. Res. 20 (3–4), 177–211.
Fischer, R., Gerya, T., 2016. Regimes of subduction and lithospheric dynamics in the Precambrian: 3D thermomechanical modelling. Gondwana Res. (submitted for publication).
Gögüs, O.H., Pysklywec, R.N., 2008a. Mantle lithosphere delamination driving plateau uplift and synconvergent extension in eastern Anatolia. Geology 36 (9), 723–726.
Gögüs, O.H., Pysklywec, R.N., 2008b. Near-surface diagnostics of dripping or delaminating lithosphere. J. Geophys. Res. Solid Earth 113 (B11), B11404.
Gerya, T., 2014a. Precambrian geodynamics: concepts and models. Gondwana Res. 25 (2), 442–463.
Gerya, T.V., 2013. Three-dimensional thermomechanical modeling of oceanic spreading initiation and evolution. Phys. Earth Planet. Inter. 214, 35–52.
Gerya, T.V., 2014b. Plume-induced crustal convection: 3D thermomechanical model and implications for the origin of novae and coronae on Venus. Earth Planet. Sci. Lett. 391, 183–192.
Gerya, T.V., Connolly, J.A.D., Yuen, D.A., Gorczyk, W., Capel, A.M., 2006. Seismic implications of mantle wedge plumes. Phys. Earth Planet. Inter. 156 (1–2), 59–74.
Gerya, T.V., Meilick, F.I., 2011. Geodynamic regimes of subduction under an active margin: effects of rheological weakening by fluids and melts. J. Metamorph. Geol. 29 (1), 7–31.
Gerya, T.V., Perchuk, L.L., Maresch, W.V., Willner, A.P., Reenen, D.D.V., Smit, C.A., 2002. Thermal regime and gravitational instability of multi-layered continental crust: implications for the buoyant exhumation of high-grade metamorphic rocks. Eur. J. Mineral. 14 (4), 687–699.
Gerya, T.V., Stern, R.J., Baes, M., Sobolev, S.V., Whattam, S.A., 2015. Plate tectonics on the Earth triggered by plume-induced subduction initiation. Nature 527 (7577), 221–225.
Gerya, T.V., Yuen, D.A., 2003. Characteristics-based marker-in-cell method with conservative finite-differences schemes for modeling geological flows with strongly variable transport properties. Phys. Earth Planet. Inter. 140 (4), 293–318.
Gerya, T.V., Yuen, D.A., 2007. Robust characteristics method for modelling multiphase visco-elasto-plastic thermo-mechanical problems. Phys. Earth Planet. Inter. 163 (1–4), 83–105.
Hansen, V.L., Willis, J.A., 1996. Structural analysis of a sampling of Tesserae: implications for Venus geodynamics. Icarus 123 (2), 296–312.
Harris, L.B., Bédard, J.H., 2014. Crustal evolution and deformation in a non-plate-tectonic Archaean Earth: comparisons with Venus. In: Evolution of Archean Crust and Early Life. Springer, pp. 215–291.
Harris, L.B., Bédard, J.H., 2015. Interactions between continent-like 'drift', rifting and mantle flow on Venus: gravity interpretations and Earth analogues. Geol. Soc. Lond. Spec. Publ. 401 (1), 327–356.
Hawkesworth, C., Kemp, A., 2006. Evolution of the continental crust. Nature 443 (7113), 811–817.
Herzberg, C., 2014. Early Earth: Archaean drips. Nat. Geosci. 7 (1), 7–8.
Herzberg, C., Condie, K., Korenaga, J., 2010. Thermal history of the Earth and its petrological expression. Earth Planet. Sci. Lett. 292 (1–2), 79–88.
Hess, P., 1989. Origins of Igneous Rocks. Harvard University Press.
Hickman, A., 2004. Two contrasting granite-greenstone terranes in the Pilbara Craton, Australia: evidence for vertical and horizontal tectonic regimes prior to 2900 Ma. Precambrian Res. 131 (3), 153–172.
Hickman, A., Van Kranendonk, M., 2004. Diapiric processes in the formation of Archaean continental crust, East Pilbara granite-greenstone terrane, Australia. The Precambrian Earth: Tempos and Events, vol. 12. Elsevier, pp. 118–139.
Hutton, J., 1788. Theory of the Earth; or an investigation of the laws observable in the composition, dissolution, and restoration of land upon the globe. Earth Environ. Sci. Trans. R. Soc. Edinburgh 1 (02), 209–304.
Ito, K., Kennedy, G.C., 1971. An experimental study of the basalt-garnet granulite-eclogite transition. In: The Structure and Physical Properties of the Earth's Crust. American Geophysical Union, pp. 303–314.
Johannes, W., 1985. The significance of experimental studies for the formation of migmatites. In: Migmatites. Springer, US, pp. 36–85 (Chapter 2).
Johnson, T.E., Brown, M., Kaus, B.J.P., VanTongeren, J.A., 2014. Delamination and recycling of Archaean crust caused by gravitational instabilities. Nat. Geosci. 7 (1), 47–52.
Katayama, I., Karato, S.-i., 2008. Low-temperature, high-stress deformation of olivine under water-saturated conditions. Phys. Earth Planet. Inter. 168 (3–4), 125–133.
Katz, R.F., Spiegelman, M., Langmuir, C.H., 2003. A new parameterization of hydrous mantle melting. Geochem. Geophys. Geosyst. 4 (9), 1073.
Kröner, A., Layer, P.W., 1992. Crust formation and plate motion in the Early Archean. Science 256 (5062), 1405–1411.
Lenardic, A., Moresi, L.N., Jellinek, A.M., Manga, M., 2005. Continental insulation, mantle cooling, and the surface area of oceans and continents. Earth Planet. Sci. Lett. 234 (3–4), 317–333.
Moore, W.B., Webb, A.A.G., 2013. Heat-pipe Earth. Nature 501 (7468), 501–505.
Moresi, L., 2013. Earth science: a resolution of the Archaean paradox. Nature 501 (7468), 496–497.
Moyen, J.-F., 2011. The composite Archaean grey gneisses: petrological significance, and evidence for a non-unique tectonic setting for Archaean crustal growth. Lithos 123 (1–4), 21–36.
O'Neill, C., Wyman, D.A., 2013. Geodynamic modeling of Late Archean subduction: pressure-temperature constraints from greenstone belt diamond deposits. In: Archean Geodynamics and Environments. American Geophysical Union, pp. 177–188 (Chapter 11).
Phillips, R.J., Hansen, V.L., 1998. Geological evolution of Venus: rises, plains, plumes, and plateaus. Science 279 (5356), 1492–1497.
Poli, S., Schmidt, M.W., 2002. Petrology of subducted slabs. Annu. Rev. Earth Planet. Sci. 30 (1), 207–235.
Ranalli, G., 1995. Rheology of the Earth. Springer.

Please cite this article in press as: Fischer, R., Gerya, T., Early Earth plume-lid tectonics: A high-resolution 3D numerical modelling approach. J. Geodyn. (2016), http://dx.doi.org/10.1016/j.jog.2016.03.004

Rey, P.F., Philippot, P., Thébaud, N., 2003. Contribution of mantle plumes, crustal thickening and greenstone blanketing to the 2.75–2.65 Ga global crisis. Precambrian Res. 127 (1–3), 43–60.
Rudnick, R.L., Gao, S., 2003. 3.01 – composition of the continental crust. In: Turekian, H.D.H.K. (Ed.), Treatise on Geochemistry. Pergamon, Oxford, pp. 1–64.
Sandiford, M., Van Kranendonk, M.J., Bodorkos, S., 2004. Conductive incubation and the origin of dome-and-keel structure in Archean granite-greenstone terrains: a model based on the eastern Pilbara Craton, Western Australia. Tectonics 23 (1).
Schaber, G.G., Strom, R.G., Moore, H.J., Soderblom, L.A., Kirk, R.L., Chadwick, D.J., Dawson, D.D., Gaddis, L.R., Boyce, J.M., Russell, J., 1992. Geology and distribution of impact craters on Venus: what are they telling us? J. Geophys. Res. Planets 97 (E8), 13257–13301.
Schmidt, M.W., Poli, S., 1998. Experimentally based water budgets for dehydrating slabs and consequences for arc magma generation. Earth Planet. Sci. Lett. 163 (1–4), 361–379.
Schutt, D.L., Lesher, C.E., 2006. Effects of melt depletion on the density and seismic velocity of garnet and spinel lherzolite. J. Geophys. Res. Solid Earth 111 (B5), B05401.
Shirey, S.B., Richardson, S.H., 2011. Start of the Wilson cycle at 3 Ga shown by diamonds from subcontinental mantle. Science 333 (6041), 434–436.
Sizova, E., Gerya, T., Brown, M., 2014. Contrasting styles of Phanerozoic and Precambrian continental collision. Gondwana Res. 25 (2), 522–545.
Sizova, E., Gerya, T., Brown, M., Perchuk, L.L., 2010. Subduction styles in the Precambrian: insight from numerical experiments. Lithos 116 (3–4), 209–229.
Sizova, E., Gerya, T., Stüwe, K., Brown, M., 2015. Generation of felsic crust in the Archean: a geodynamic modeling perspective. Precambrian Res. 271, 198–224.
Smithies, R.H., Champion, D.C., Van Kranendonk, M.J., 2009. Formation of Paleoarchean continental crust through infracrustal melting of enriched basalt. Earth Planet. Sci. Lett. 281 (3–4), 298–306.
Strom, R., Schaber, G., Dawson, D., 1994. The global resurfacing of Venus. J. Geophys. Res. 99 (E5), 10,899–10,926.
Turcotte, D., Schubert, G., 2002. Geodynamics, 2nd ed. Cambridge University Press.
Ueda, K., Gerya, T., Sobolev, S.V., 2008. Subduction initiation by thermal–chemical plumes: numerical studies. Phys. Earth Planet. Inter. 171 (1–4), 296–312.
van Hunen, J., Moyen, J.-F., 2012. Archean subduction: fact or fiction? Annu. Rev. Earth Planet. Sci. 40 (1), 195–219.
van Hunen, J., van den Berg, A.P., 2008. Plate tectonics on the early Earth: limitations imposed by strength and buoyancy of subducted lithosphere. Lithos 103 (1–2), 217–235.
Van Kranendonk, M.J., 2010. Two types of Archean continental crust: plume and plate tectonics on early Earth. Am. J. Sci. 310 (10), 1187–1209.
Van Kranendonk, M.J., 2011a. Cool greenstone drips and the role of partial convective overturn in Barberton greenstone belt evolution. J. Afr. Earth Sci. 60 (5), 346–352.
Van Kranendonk, M.J., 2011b. Onset of plate tectonics. Science 333 (6041), 413–414.
Van Kranendonk, M.J., Collins, W., Hickman, A., Pawley, M.J., 2004. Critical tests of vertical vs. horizontal tectonic models for the Archaean East Pilbara granite-greenstone terrane, Pilbara craton, western Australia. Precambrian Res. 131 (3), 173–211.
Van Kranendonk, M.J., Kröner, A., Hoffmann, J.E., Nagel, T., Anhaeusser, C.R., 2014a. Just another drip: re-analysis of a proposed Mesoarchean suture from the Barberton Mountain Land, South Africa. Precambrian Res. 254, 19–35.
Van Kranendonk, M.J., Smithies, R.H., Griffin, W.L., Huston, D.L., Hickman, A.H., Champion, D.C., Anhaeusser, C.R., Pirajno, F., 2014. Making it thick: a volcanic plateau origin of Palaeoarchean continental lithosphere of the Pilbara and Kaapvaal cratons. Geol. Soc. Lond. Spec. Publ. 389.
Van Kranendonk, M.J., Smithies, R.H., Hickman, A.H., Champion, D.C., 2007. Chapter 4.1. Paleoarchean development of a continental nucleus: the East Pilbara Terrane of the Pilbara Craton, Western Australia. In: Martin, J., van Kranendonk, R.H.S., Vickie, C.B. (Eds.), In: Developments in Precambrian Geology, vol. 15. Elsevier, pp. 307–337.
van Thienen, P., van Summeren, J., Van der Hilst, R., Van den Berg, A., Vlaar, N., 2005. Numerical study of the origin and stability of chemically distinct reservoirs deep in Earth's mantle, Geophysical monograph.
van Thienen, P., Vlaar, N.J., van den Berg, A.P., 2005b. Assessment of the cooling capacity of plate tectonics and flood volcanism in the evolution of Earth, Mars and Venus. Phys. Earth Planet. Inter. 150 (4), 287–315.
Zegers, T.E., van Keken, P.E., 2001. Middle Archean continent formation by crustal delamination. Geology 29 (12), 1083–1086.
Zhu, G., Gerya, T.V., Tackley, P.J., Kissling, E., 2013. Four-dimensional numerical modeling of crustal growth at active continental margins. J. Geophys. Res. Solid Earth 118 (9), 4682–4698.

Please cite this article in press as: Fischer, R., Gerya, T., Early Earth plume-lid tectonics: A high-resolution 3D numerical modelling approach. J. Geodyn. (2016), http://dx.doi.org/10.1016/j.jog.2016.03.004